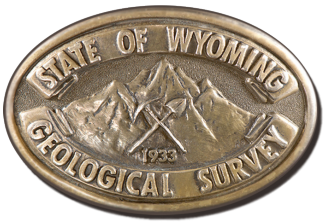

Interpreting the past, providing for the future

Heavy-Mineral Sandstone in the Upper Cretaceous Rock Springs Formation, Richards Gap, Wyoming

Derek T. Lichtner, Garrett W. Gay, and Kelsey S. Kehoe

Open File Report 2021-6
July 2021

Wyoming State Geological Survey

Erin A. Campbell, Director and State Geologist

Heavy-Mineral Sandstone in the Upper Cretaceous Rock Springs Formation, Richards Gap, Wyoming

Derek T. Lichtner, Garrett W. Gay, and Kelsey S. Kehoe

Layout by James R. Rodgers

Open File Report 2021-6
Wyoming State Geological Survey
Laramie, Wyoming: 2021

Citation: Lichtner, D.T., Gay, G.W., and Kehoe, K.S., 2021, Heavy-mineral sandstone in the Upper Cretaceous Rock Springs Formation, Richards Gap, Wyoming: Wyoming State Geological Survey Open File Report 2021-6, 37 p.

Table of Contents

List of Figures

ABSTRACT

This study is a preliminary examination of geochemical data collected from a heavy-mineral sandstone, or paleoplacer, in the McCourt Sandstone Tongue of the Rock Springs Formation during mapping of the bedrock geology of the Richards Gap 7.5' quadrangle in southwestern Wyoming. Sample analyses indicate the presence of several critical mineral resources, of which the most notable are abundant titanium, zirconium, and rare earth elements, as well as elevated hafnium, niobium, and vanadium. Diagenetic alteration of the deposit appears to have locally enhanced enrichment of these elements. However, the economic potential of the deposit is compromised by substantial induration, which can hinder conventional disaggregation methods for this type of deposit; uncertainty regarding the presence of titanium-bearing phases that may complicate ore processing; limited volume of exposure due to dipping strata, erosion, and burial; and uncertainty regarding the extent of diagenetic alteration. Further work is needed to explore how these factors might influence the mineralogy and economic potential of this deposit and other Upper Cretaceous heavy-mineral sandstones in Wyoming.

INTRODUCTION

Critical Minerals

The U.S. Geological Survey (USGS) defines a critical mineral as one that is essential for advanced technology and national defense applications, and whose global supply chain is at risk of disruption. The USGS's list of 35 critical minerals, first published in 2017 (Schulz and others, 2017a), and expanded and finalized in 2018 (Fortier and others, 2018), includes many critical mineral resources that have known or potential sources in Wyoming.

The heavy-mineral-sand-type deposit investigated in this study is most commonly associated with titanium (Ti), zirconium (Zr), and the rare earth elements (REEs). Titanium metal and alloys are used in the aerospace industry, biomedical implants, and various other products because of their resistance to corrosion and high strength-to-weight ratio (Woodruff and others, 2017). In addition, because of its high refractive index, titanium dioxide is extensively used as a white pigment (Woodruff and others, 2017). Zirconium metal is used in applications requiring resistance to corrosion and high temperatures, as well as specific neutron-absorption properties, mainly in the ceramics, chemical, and nuclear energy industries (Jones and others, 2017). The REEs consist of the 14 naturally occurring lanthanide metals—lanthanum (La), cerium (Ce), praseodymium (Pr), neodymium (Nd), samarium (Sm), europium (Eu), gadolinium (Gd), terbium (Tb), dysprosium (Dy), holmium (Ho), erbium (Er), thulium (Tm), ytterbium (Yb), and lutetium (Lu)—which all share similar chemical properties. Scandium (Sc) and yttrium (Y) are also often grouped with the REEs because they too have these properties; in this report, "REEs" refers to all 16 of these elements. The REEs are used in a wide array of applications, including specialty glass products, permanent magnets, steelmaking, batteries, and various other electronic components (Van Gosen and others, 2017).

Heavy-Mineral Sands

For the purposes of this study, a "heavy mineral" is an accessory detrital mineral with high density relative to quartz (2.65 g/cm^3) and feldspar (2.54–2.76 g/cm^3), the two primary components of siliciclastic sands and sandstones. Typically, heavy minerals comprise only a minor fraction (less than one percent) of the mineral assemblage. However, because of their high density, heavy minerals are subject to mechanical sorting during erosion and transport. A placer deposit can form if sedimentological processes produce a significant accumulation of concentrated heavy minerals.

Coastal heavy-mineral sands, or beach placers, sometimes called "black sands," are the world's primary source for titanium (Woodruff and others, 2017). Ninety percent of the world's zirconium is also produced from heavy-mineral sand deposits (Van Gosen and Ellefsen, 2018). REEs and thorium (Th) are commonly recovered

as byproducts in titanium and zirconium mining operations (Van Gosen and others, 2019). Most heavy-mineral sand deposits currently mined are Quaternary, Neogene, or Paleogene in age; are unconsolidated or poorly consolidated; and contain heavy-mineral concentrations of at least 2 percent (Van Gosen and others, 2014). Numerous studies exist on younger heavy-mineral sand deposits in Australia, the Atlantic Coastal Plain of the United States, India, South Africa, and elsewhere. For an introduction to this body of work, see Van Gosen and others (2014), Hou and others (2017), and Van Gosen and Ellefsen (2018).

Heavy-mineral sands that are Upper Cretaceous in age are found throughout the Rocky Mountain region. These deposits are associated with littoral-type regressive sandstones that were deposited along the margin of the Western Interior Seaway (Houston and Murphy, 1977). They differ from younger, currently mined titaniferous heavy-mineral sand deposits in that they are often lithified. Previously published analyses indicate Cretaceous deposits in Wyoming may contain up to 59 percent heavy minerals, 1.6 to 33.9 percent titanium oxide (TiO_2), and 1.4 to 4.8 percent zirconium oxide (ZrO_2; Dow and Batty, 1961; Houston and Murphy, 1962; Madsen, 1978; Hausel, 1990). Where comprehensive geochemical data exist, Cretaceous heavy-mineral sand deposits are sometimes also enriched in hafnium (Hf), niobium (Nb), vanadium (V), thorium (Th), and REEs (Sutherland and Cola, 2016).

One such Upper Cretaceous heavy-mineral sand deposit was sampled and analyzed during Wyoming State Geological Survey (WSGS) mapping of the Richards Gap 1:24,000-scale quadrangle in southwestern Wyoming, in cooperation with the USGS 2020 STATEMAP grant award G20AC00199 (Kehoe and others, 2021). This report is a brief summary of data collected at Richards Gap and the preliminary results.

Richards Gap Heavy-Mineral Sand Deposit

Previous work

The first known description of a heavy-mineral sand deposit in the study area was by Murphy and Houston (1955). They describe a heavy-mineral sandstone at the base of the Ericson Sandstone in the Richards Gap quadrangle, which they name the Red Creek deposit. They report that altered ilmenite comprises 85 to 90 percent of the non-ferromagnetic heavy-mineral fraction.

Dow and Batty (1961), in their reconnaissance of heavy-mineral sands in the Rocky Mountain region, provide abbreviated geochemical analyses of several heavy-mineral sandstones in southwestern Wyoming, including the Red Creek deposit. Analysis of four samples yielded a range of compositions. The highest-grade sample exhibited 32 percent TiO_2, 27.5 percent iron (Fe), and 2.2 percent ZrO_2, whereas the lowest grade sample contained 9.4 percent TiO_2, 8 percent Fe, and 0.4 percent ZrO_2.

Houston and Murphy (1962) present additional geochemical data as well as petrographic analysis in their overview of known titaniferous black sandstones in Wyoming. For three samples, they report an average heavy-mineral fraction of 27.5 percent, with a range of 4.8 to 44.7 percent. Of the heavy-mineral fraction, they report an average of 82.8 percent opaque minerals, 13.7 percent zircon, 2.4 percent garnet, one percent tourmaline, one percent rutile, and trace amounts of biotite, epidote, chlorite, staurolite, and monazite. Geochemical analysis of eight samples yielded an average TiO_2 content of 14.05 percent, with a range of 0.16 to 36.5 percent, and an average iron oxide (Fe_2O_3) concentration of 19.09 percent, with a range of 2.65 to 42.34 percent. Several years later, in a pioneering study on detrital zircon techniques, Houston and Murphy (1965) used the lead-alpha method to date two detrital zircon grains, one of which was from the Red Creek deposit with an age of 770 ± 80 Ma. Houston and Murphy again refer to the Red Creek deposit in their expanded summary of black sandstones in the Rocky Mountain region (Houston and Murphy, 1970) and in their depositional model of Upper Cretaceous heavy-mineral sand deposition throughout the region (Houston and Murphy, 1977).

Roehler (1989) published the definitive work on the stratigraphy and sedimentology of Upper Cretaceous heavy-mineral sands in the Rock Springs Uplift. In this study, Roehler described six deposits, measured numerous stratigraphic sections, devised a detailed depositional model, and compared the model to Holocene analogs. Roehler renamed the Red Creek deposit of previous researchers the Richards Gap deposit and placed it within the McCourt Sandstone Tongue of the Rock Springs Formation, not the Ericson Sandstone.

In the 1990s and 2000s, several mineral-resources reports mention the Richards Gap heavy-mineral sand deposit and occasionally provide commentary on the existing data (King and Harris, 1987; Hausel, 1990; King, 1991; Force, 2000; Force and others, 2001). No additional data are known until Sutherland and Cola's (2016) report on REE-bearing minerals in Wyoming, in which they provide a comprehensive geochemical analysis, including REEs and other trace elements, for one grab sample from Richards Gap. Elevated concentrations in the sample include 33.9 percent TiO_2, 44.2 percent Fe_2O_3, 785 parts per million (ppm; 10,000 ppm is 1 percent) Hf, 434 ppm Nb, 1,200 ppm V, >10,000 ppm Zr, and 2,340 ppm total REEs, including Sc and Y.

Geologic setting

Within the study area, the Upper Cretaceous (Campanian) Rock Springs Formation is an 80-m-thick (295 ft) package of sandstone and shale with minor carbonaceous shale and coal. At Richards Gap, the McCourt Sandstone Tongue of the Rock Springs Formation is a laterally continuous tan and white bench-forming sandstone. The underlying Coulson Tongue is drab gray marine shale, and the overlying Gottsche Tongue consists of coastal-plain carbonaceous shale, coal, and sandstone. A large number of Upper Cretaceous strata throughout Wyoming, including the Rock Springs Formation, were deposited in or marginal to the Western Interior Seaway, in the Sevier foreland basin. Sediment sourced from the Sevier orogenic belt to the west was transported by rivers to the coast, where it was reworked by storms, waves, and longshore currents (Roehler, 1989; Minor and others, 2021).

The Rock Springs Formation at Richards Gap is exposed where Red Creek cuts through hogback ridges of resistant Mesaverde Group sandstones on the north-dipping southerly limb of the Red Creek syncline, which separates the Rock Springs Uplift from the Uinta Mountains (fig. 1) To the north, the heavy-mineral sand deposit plunges beneath and is covered by the overlying Gottsche Tongue and the Ericson Sandstone. To the south, the southerly limb of the Red Creek syncline becomes the northerly limb of the Clay Basin anticline (Hansen, 1957), and at the northern margin of Clay Basin, a topographic depression formed at the center of this anticline, the deposit has been eroded.

Location and outcrop

The Richards Gap heavy-mineral sand deposit (fig. 2) is in Sweetwater County, Wyoming, in SE1/4 sec. 22, T. 12 N., R. 105 W., along Clay Basin Road (County Road 62), about 450 m (1,480 ft) north of the Wyoming-Utah border. The westernmost exposure is located in a steep, shallow gully about 95 m (310 ft) east of and 20 m (65 ft) above the road. The exposure curves around the back of the gully and climbs up along the crest of the ridge to the southeast for 650 m (2,130 ft) before pinching out about 120 m (390 ft) above the road elevation. The deposit is visible from Clay Basin Road as a dark-brown band near the ridge top (fig. 3). The sandstones in the McCourt Sandstone Tongue that immediately underlie the heavy-mineral sand deposit, typically buff to white in color, are here stained rusty brown.

The deposit is thickest at its western end, with a maximum thickness of 2.1 m (6.9 ft) at the back of the aforementioned gully (fig. 4). Pinch out between here and the road occurs rapidly, within 50 m (160 ft). To the east, the deposit is relatively thick for another 100 m (330 ft), after which it thins to less than 1 m (3 ft). For the remaining 500 m (1,640 ft) of exposure to the east, the deposit pinches and swells (fig. 5), varying in thickness from 0.1 m (0.3 ft) to 0.6 m (2 ft), before pinching out. Bedding is indistinct within much of the deposit. Where the deposit is thickest, the upper 1 m (3 ft) tends to break into flaggy, fist-sized pieces.

Depositional environment

Based on lithofacies analysis of nine measured sections at Richards Gap and 47 stratigraphic sections at other heavy-mineral sand locations in the Rock Springs Uplift, Roehler (1989) created a depositional model for heavy-mineral sand deposition in the McCourt Sandstone Tongue. Sedimentological process along the McCourt coast was wave-dominated, with prominent longshore currents to the southwest. River drainages originated in the Sevier orogenic belt to the west and contributed sediment to the shoreline. Tides do not appear to have had a major influence on McCourt Sandstone Tongue deposition. The majority of heavy-mineral sand deposits in the McCourt Sandstone Tongue were deposited in upper shoreface, surf-dominated environments. The Richards Gap deposit is unique in that facies analysis indicates it was deposited at the mouth of a small river; strong longshore currents and waves reworked the river-sourced sediment.

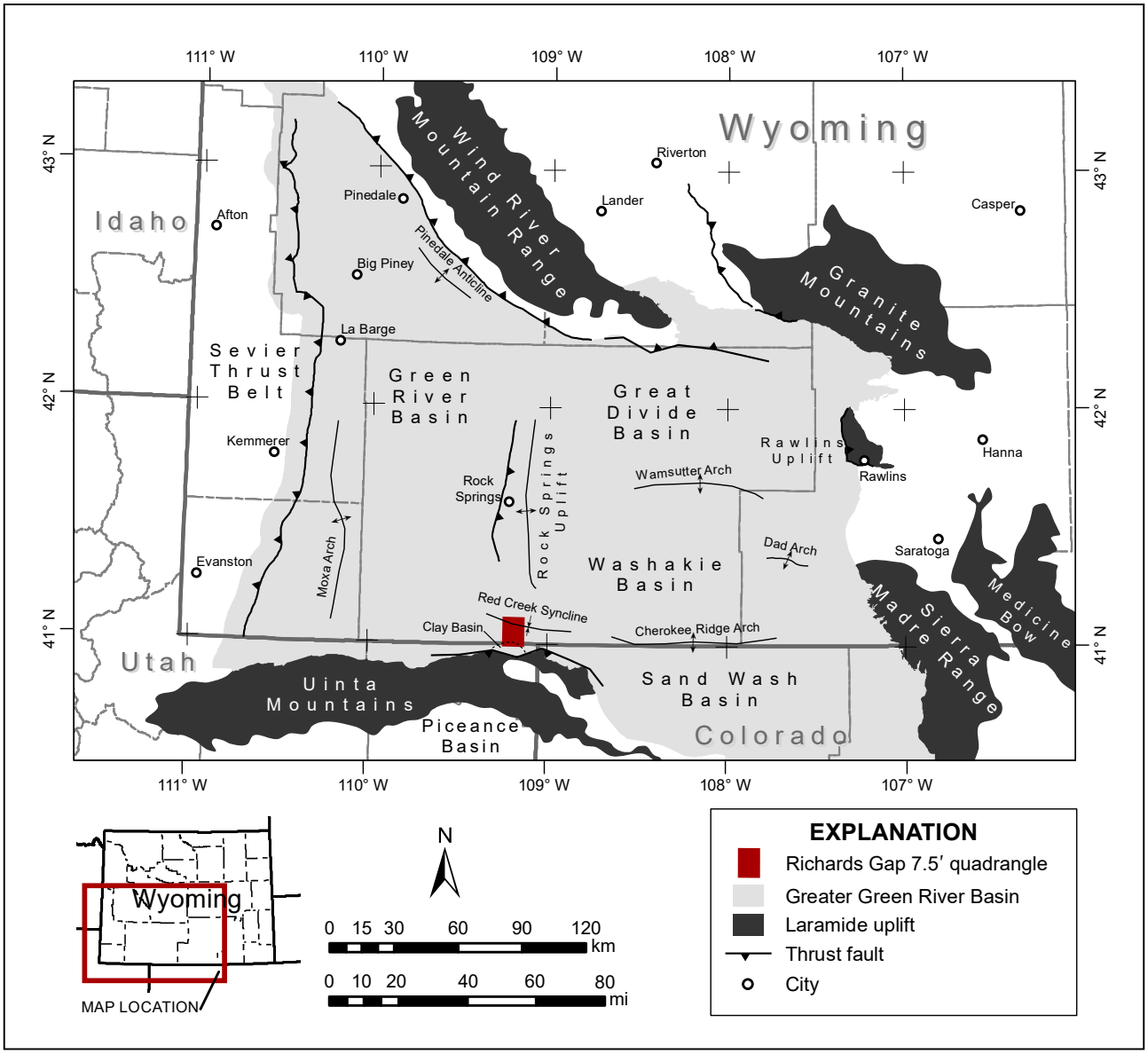

Figure 1. Map of the Greater Green River Basin in southwestern Wyoming and adjacent states, showing the locations of the Richards Gap 7.5' quadrangle (Kehoe and others, 2021) and regional geologic structures.

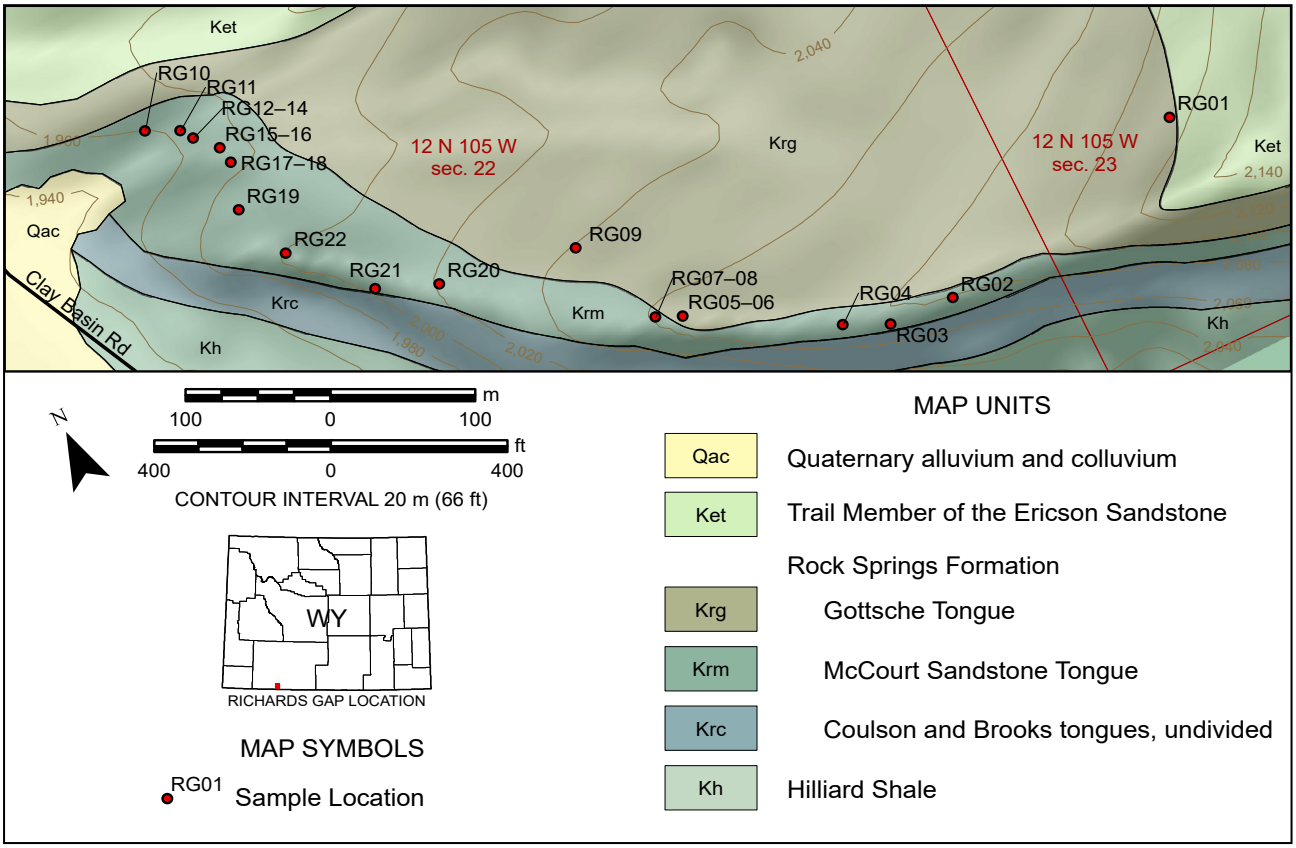

Figure 2. Bedrock geologic map and sample locations for the heavy-mineral sand deposit at Richards Gap. Modified from the 1:24,000-scale bedrock geologic map of the Richards Gap 7.5' quadrangle by Kehoe and others (2021).

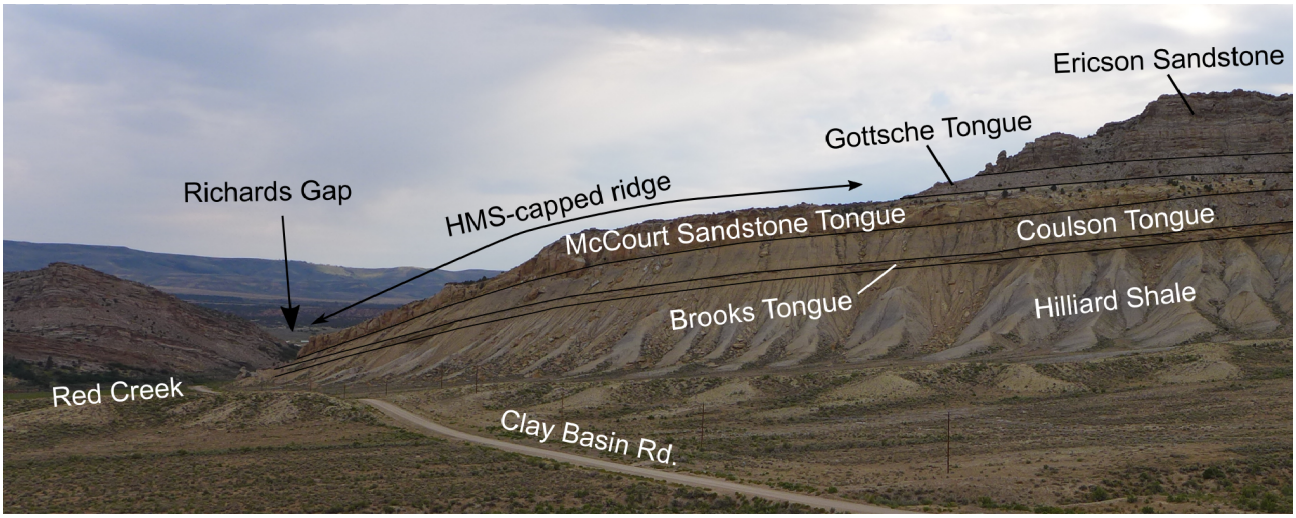

Figure 3. Photo of Richards Gap and adjacent resistant ridges of Mesaverde Group. View is to the north, from Clay Basin. The Richards Gap heavy-mineral sand deposit caps the top of this ridge for a distance of about 800 m (2,620 ft) along strike.

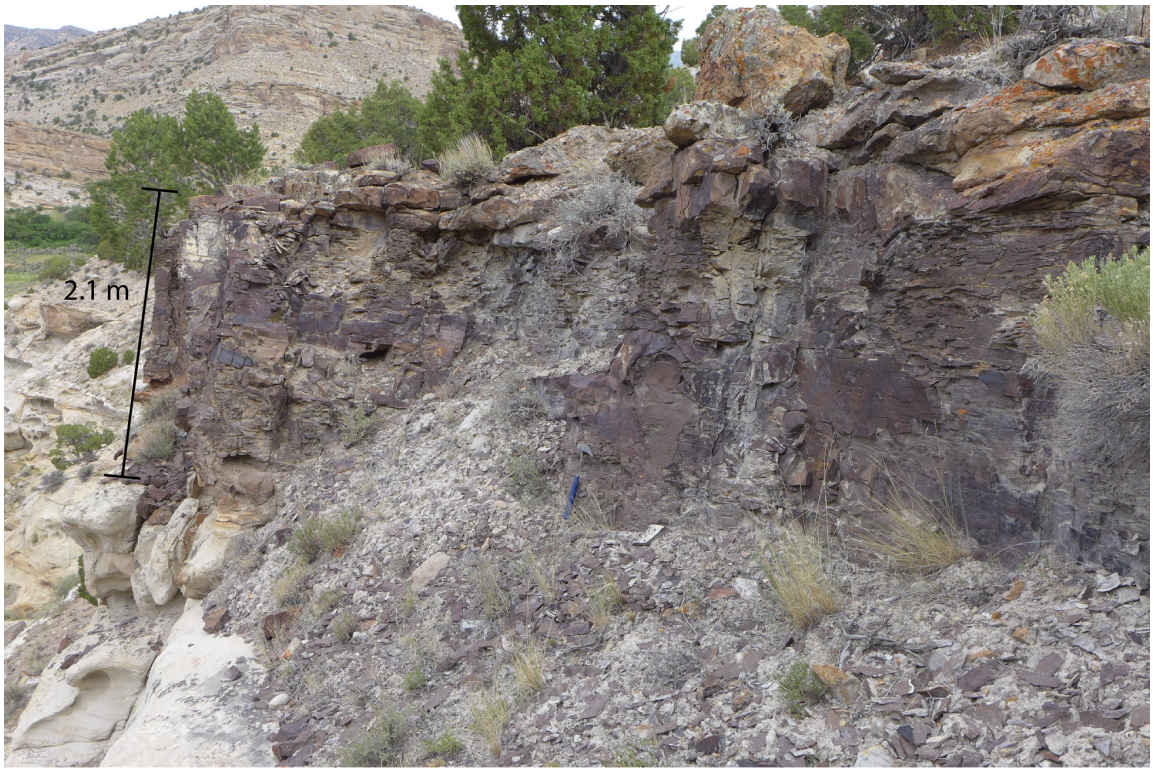

Figure 4. Photo of the thickest portion of the heavy-mineral sand deposit at Richards Gap, from sampling location of RG15 and RG16. View is to the northwest, toward sampling location of RG12, RG13, and RG14.

Figure 5. Photo of the heavy-mineral sand deposit near its easternmost extent. View is to the southwest, with Red Creek in the background.

METHODS

Sample Collection

Twenty-two sandstone samples were collected from the McCourt Sandstone and Gottsche tongues at Richards Gap. Sampling locations were established approximately every 25–100 m (85–330 ft) along strike, depending on the quality of exposure (fig. 6). Several samples were collected at each location, or, where the heavy-mineral sand deposit was less than 0.5 m (1.5 ft) thick, a single representative sample was collected. Background samples were also collected from laterally adjacent or overlying littoral and fluvial sandstones with no apparent heavy-mineral enrichment.

The 15 samples designated as heavy-mineral sands, or HMS, in the tables and figures of this report are those samples that, based on qualitative indicators in the field, such as color, induration, relative density, visible mineralogy, and stratigraphic location, were considered part of the heavy-mineral sand deposit (Appendix 1). Seven additional samples were collected from laterally or stratigraphically adjacent parts of the McCourt and Gottsche tongues.

Sample Analysis

The geochemistry of each sample, with a focus on trace and rare earth elements, was analyzed using a combination of laboratory methods. Samples were prepared for whole rock analyses (major element oxides) by lithium borate fusion and measured with X-ray fluorescence (XRF; Appendix 2). Samples were prepared for trace element analyses by sodium peroxide fusion and measured with inductively coupled plasma mass spectrometry (ICP-MS; Appendix 3). Trace metal samples were prepared with acid digestion and measured with ICP optical emission spectrometry (ICP-OES); the relative insolubility of many REE-bearing minerals should be kept in mind when interpreting the results of this method (Appendix 4). Lastly, samples were prepared for analyzing gold (Au), platinum (Pt), and palladium (Pd) levels by fire assay and measured with ICP-OES (Appendix 5). Sample preparation and analysis for this project was conducted by AGAT Laboratories of Ontario, Canada.

Additional analytical methods were performed at the WSGS laboratory in Laramie, Wyoming, including reflected- and refracted-light microscopy, and powder X-ray diffraction (XRD). XRD results are preliminary and not reported here; however, they were used to aid in identification of mineral phases. Reflected-light photomicrographs are reproduced in Appendix 6.

RESULTS

Titanium

Of the 15 heavy-mineral sandstone samples collected at Richards Gap, whole rock TiO_2 concentrations spanned a wide range, from 0.22 percent to 40.4 percent, with an average of 19.7 percent (fig. 7; 1 percent TiO_2 is 0.6 percent Ti). In comparison, the seven background sandstone samples exhibited TiO_2 concentrations in the range of 0.04 percent to 0.14 percent. For reference, heavy-mineral sand deposits currently mined in other parts of the world contain about 1–3 percent TiO_2 (Woodruff and others, 2017); despite their relatively low TiO_2 content, such deposits are economically viable because of favorable mineralogy (abundant rutile [TiO_2], or high Ti/Fe ratio) and ease of extraction. In contrast, igneous ores for Ti, which present challenges in mining and processing, usually contain TiO_2 in the range of 11 to 18 percent (Woodruff and others, 2017).

Preliminary examination of thin sections under reflected light reveals an abundance of subrounded to rounded ilmenite ($FeTiO_3$) that has experienced varying degrees of alteration. Titanium in the samples may also occur within an ilmenite-hematite solid solution mineral (variously named ferrian ilmenite, titanohematite, or hemo-ilmenite) often found in Mesozoic sandstones of the western United States and sometimes mistaken for magnetite (Force and others, 2001); the relatively elevated Fe within this Ti-bearing mineral, if indeed present,

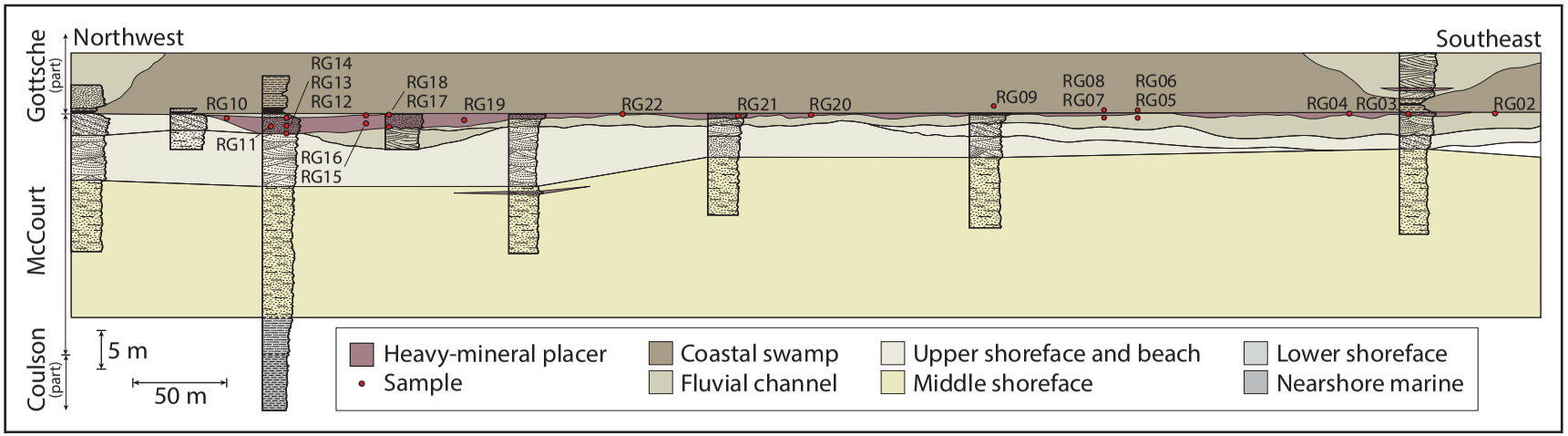

Figure 6. Cross section of the McCourt Sandstone Tongue at Richards Gap showing sample locations, lithologies, and depositional environments. Measured sections modified from Roehler (1989). Lithologic symbols are FGDC standard symbology (U.S. Geological Survey, 2006).

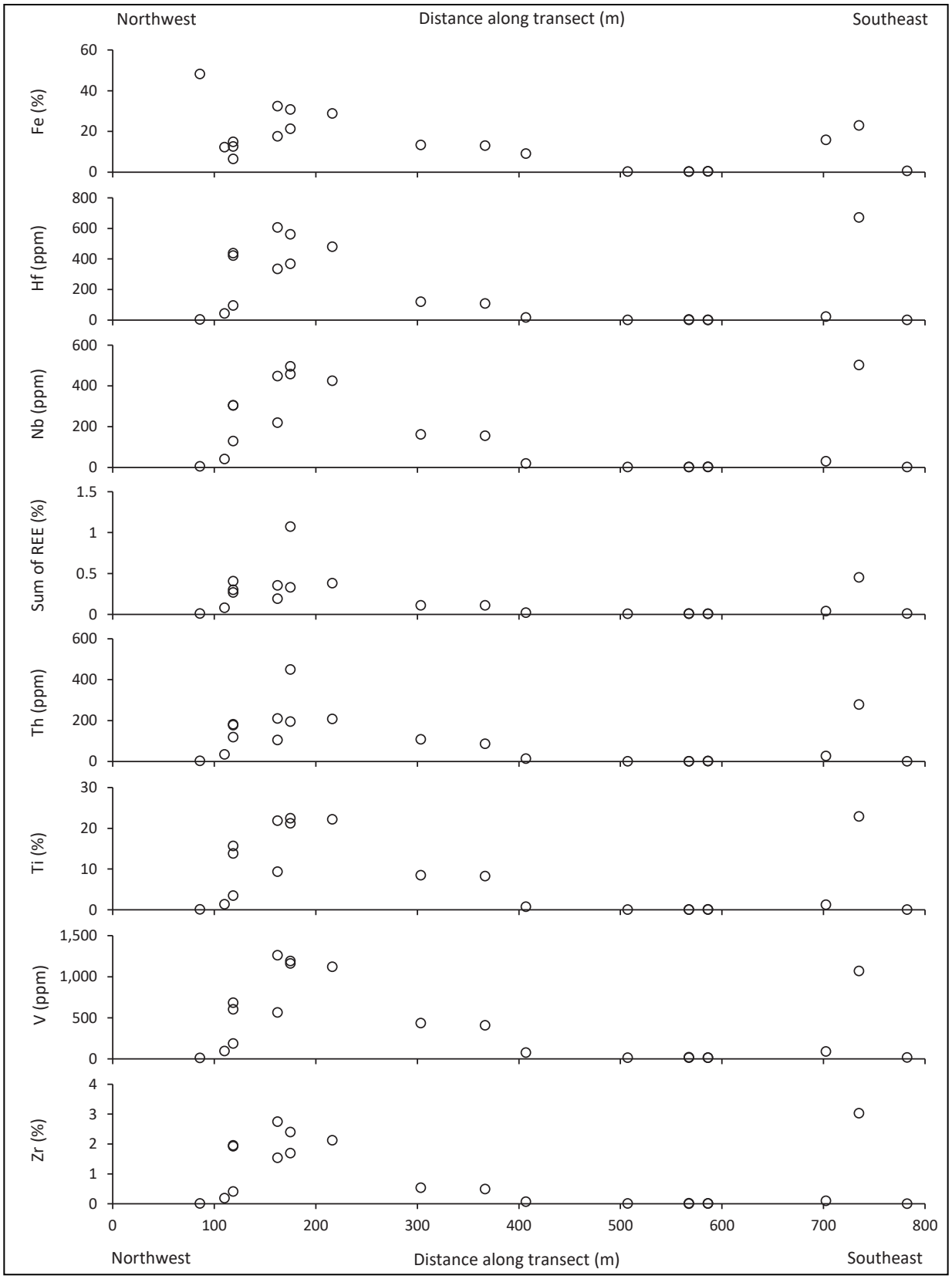

Figure 7. Geochemical data for elements of interest in the Richards Gap heavy-mineral sand deposit, plotted spatially along the x-axis from the northwest (left) to the southeast (right) exposure.

would lower the quality of the Ti ore. Economic ilmenite concentrates typically contain less than 14 percent Fe as Fe_2O_3 and about 10 to 20 percent FeO. Elevated Fe levels also have a detrimental effect on the color of TiO_2 pigment (Perks and Mudd, 2019).

In the samples with greatest Ti-enrichment, the ilmenite appears heavily altered and pitted, and surrounded by amorphous and microcrystalline leucoxene intergrowths (Appendix 6, figs. A6-8 and A6-11). The altered samples also have elevated Ti/Fe ratios, suggesting dissolution and removal of Fe, upgrading their Ti content (Woodruff and others, 2017; Perks and Mudd, 2019). Preliminary powder-XRD measurements indicate that anatase (TiO_2) is the primary Ti-bearing mineral phase in these heavily altered samples. In contrast, several samples identified in the field as heavy-mineral sand ore based on qualitative indicators such as color were only modestly enriched in Ti, Zr, REEs, and other elements of interest; instead, these samples showed elevated Fe.

Zirconium

Elemental Zr concentrations in the Richards Gap heavy-mineral sand samples range from 145 ppm to 3.03 percent, with an average of 1.28 percent (fig. 7). The background sandstone samples exhibited Zr concentrations of 36.4 ppm to 179 ppm, with an average of 81.2 ppm. Zircon ($ZrSiO_4$) is readily identifiable in the heavy-mineral sand samples. At least two distinct populations of zircon can be observed in thin section: abundant pink well-rounded zircons and occasional colorless euhedral zircons. The Zr concentrations in the Richards Gap deposit are elevated and on the higher-end of known measurements for Cretaceous heavy-mineral sands in the region (Dow and Batty, 1961).

Rare Earth Elements

In the heavy-mineral sand samples, cumulative total REE concentrations, including Sc and Y, ranged from 118 ppm to 1.07 percent, averaging about 2,750 ppm. All REEs were elevated compared to their average crustal abundance (fig. 8; Taylor and McLennan, 1985). The light REEs, or LREEs (La, Ce, Pr, Nd, Sm), showed the greatest enrichment, typically greater than ten times each element's crustal abundance, and as great as 94 times the crustal abundance in the highest grade sample (Taylor and McLennan, 1985). The heavy REEs, or HREEs (Eu, Gd, Tb, Dy, Ho, Er, Tm, Yb, Lu), also displayed elevated concentrations, on average about five to seven times the crustal abundance, with a maximum of 34 times the crustal abundance. In contrast, the background samples yielded an average REE total of 93 ppm, and the average concentration of any individual REE was less than its average crustal abundance.

The REEs in the Richards Gap deposit are contained within the minerals monazite ($[LREE,Th]PO_4$) and xenotime ($[Y,HREE,Th,U]PO_4$). The greatest total REE concentrations were observed in those samples that also showed significant alteration of ilmenite to anatase leucoxene. Further work is required to examine how diagenetic processes might enhance or inhibit REE-enrichment in the McCourt Sandstone Tongue and similar deposits.

REE minerals in heavy-mineral sand deposits are typically byproducts of Ti and Zr mining operations, on which the economic feasibility of such a deposit relies. In contrast, igneous REE ores, such as carbonatite intrusions, have average rare earth oxide (REO) contents of several percent (Van Gosen and others, 2019). For example, the Mountain Pass deposit in southern California has an average grade of 7.98 percent REO (about 6.7 percent REEs), and the Bear Lodge carbonatite in northeastern Wyoming averages 2.78 percent REO (about 2.4 percent REEs).

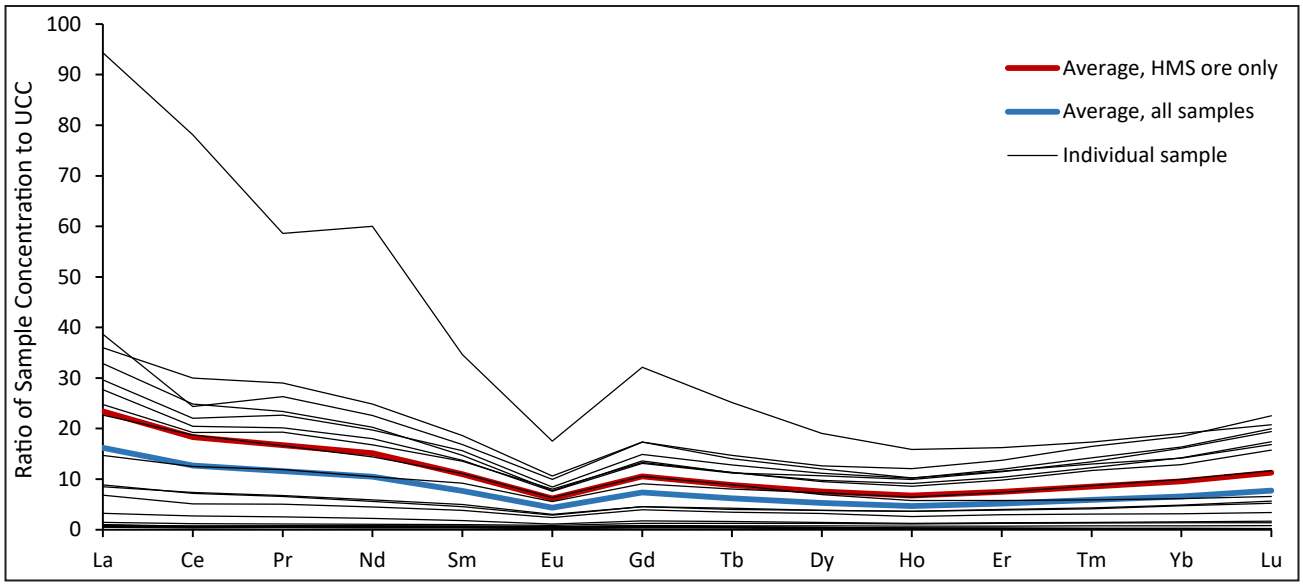

Figure 8. REE concentrations normalized by their average abundance in the upper continental crust (UCC; Taylor and McLennan, 1985) for samples examined in this study. "HMS ore" are those samples that, based on qualitative assessment of color, density, and mineralogy in the field, agreed with previously published descriptions of the HMS deposit (Houston and Murphy, 1962; Roehler, 1989). Non-ore samples plotted together near or below average crustal abundance.

Other Elements of Interest

Hafnium

Hafnium (Hf), also a critical mineral, not only shares many chemical properties and industrial uses with zirconium but also occurs in similar geologic contexts (Jones and others, 2017). Concentrations in the Richards Gap heavy-mineral sand deposit ranged from 4 ppm to 672 ppm Hf, averaging about 287 ppm. Background samples averaged 2 ppm Hf.

Niobium

Niobium concentrations in the Richards Gap heavy-mineral sand deposit ranged from 5 ppm to 503 ppm, with an average of 246 ppm. The background sandstone samples exhibited Nb concentrations less than 3 ppm. Nb is commonly associated with pyrochlore ($[Na,Ca,Ce]_2[Nb,Ti,Ta]_2[O,OH,F]_7$) and columbite ($[Fe,Mn][Nb,Ta]_2O_6$) group minerals in carbonatite and alkaline igneous rocks and associated placer deposits (Schulz and others, 2017b), as well as with Ti-bearing minerals (Fleischer and others, 1952; Bingler, 1963). Houston and Murphy (1970) indicate the presence of an unidentified Nb-bearing opaque mineral in Cretaceous-age placer deposits similar to the Richards Gap deposit. Moderately elevated tantalum (Ta) and tungsten (W) in the Nb-enriched Richards Gap samples suggest the presence of columbite group minerals. Most of the world's niobium is mined from carbonatite or weathered-carbonatite ores, in which Nb concentrations tend to range from 350 ppm to 1 percent (0.1 to 3 percent Nb_2O_5; Schulz and others, 2017b). Niobium impurities in ilmenite concentrates can affect the color of end-product TiO_2 pigment and produce toxic waste materials in sulfate-route pigment production (Perks and Mudd, 2019).

Precious metals

The Richards Gap heavy-mineral sand samples did not contain significant levels of Au, Pt, or Pd. Silver (Ag) was somewhat elevated, with a maximum concentration of 8 ppm, compared to an average crustal abundance of 0.05 ppm (Taylor and McLennan, 1985). In contrast, the average grade of known volcanogenic massive sulfide deposits is 33 ppm Ag (Graybeal and Vikre, 2010).

Thorium

The samples show moderately elevated levels of Th, as high as 450 ppm. In heavy-mineral sand deposits, Th is typically contained with the REE-bearing mineral monazite. Although Th is not considered a critical mineral commodity by the USGS, Th ore is considered a "Source Material" by the U.S. Nuclear Regulatory Commission (2021). Scintillation-counter measurements taken at the heavy-mineral sand deposit showed radiation levels several times that of background. If a heavy-mineral sand is mined primarily for Ti or Zr, significant concentrations of Th in monazite could complicate operations by producing potentially radioactive waste materials (Woodruff and others, 2017).

Vanadium

Like Nb, V is associated with Ti-bearing minerals (Schuiling and Feenstra, 1980). Concentrations in the Richards Gap heavy-mineral sand ranged from 12 ppm to 1,260 ppm V, averaging 597 ppm. Background samples averaged 15 ppm V.

Vanadium production worldwide is usually from igneous ores, primarily vanadiferous titanomagnetite deposits (Kelley and others, 2017), not from heavy-mineral sand placers. U.S. domestic production is primarily from sandstone-hosted uranium and vanadium deposits in the Colorado Plateau. A typical ore of either variety has average grades of at least 280 ppm to greater than 2,800 ppm V (0.1 to 1 percent V_2O_5; Kelley and others, 2017). Like Nb, high V concentrations in ilmenite ore can affect the color of TiO_2 pigment and produce toxic waste materials (Perks and Mudd, 2019).

Spatial Distribution of Critical Minerals

With the exception of one sample, heavy-mineral enrichment in the Richards Gap deposit is limited to the western 400 m (1,312 ft) of the deposit (fig. 7). In particular, a 150-m-wide (490 ft) zone, corresponding to the thickest part of the deposit, contains concentrations of the elements of interest that are orders of magnitude greater than elsewhere in the McCourt Sandstone Tongue at Richards Gap.

Within the thick enriched zone, heavy minerals become increasingly common upward, reflecting the mechanical sorting process along the Cretaceous shoreline. While the grain size of a typical quartz-rich, prograding shoreline deposit coarsens upward, the Richards Gap deposit fines upwards, as the sediment, being of non-uniform composition, was sorted by density, not size.

CONCLUSION

Various factors influence the critical mineral potential of the Richards Gap heavy-mineral sand deposit. In the deposit's favor are its significantly elevated Ti, Zr, and REE concentrations. The Ti and Zr concentrations presented in this report are among the highest known in Cretaceous-age heavy-mineral sands throughout the region (Dow and Batty, 1961; Houston and Murphy, 1962; Sutherland and Cola, 2016) and are more than an order of magnitude greater than typically mined heavy-mineral sand ores (Jones and others, 2017; Woodruff and others, 2017). REE concentrations are likewise high. Diagenetic alteration at Richards Gap, in addition to the mechanical sorting process during deposition, appears to have further enriched the deposit in critical minerals.

However, the economic potential of the deposit at Richards Gap is limited or made uncertain by several factors. The deposit is well-indurated, unlike typically mined heavy-mineral sand ores, which are unconsolidated to poorly consolidated, preventing the usual methods of mineral separation (Perks and Mudd, 2019). In addition, the volume of the deposit at Richards Gap is compromised by erosion to the south and burial under younger, moderately dipping formations to the north. Furthermore, the occurrence of significant quantities of Ti within an ilmenite-hematite solid solution mineral—the presence of which is suspected but not confirmed—would

complicate Ti recovery with conventional methods (Force and others, 2001; Perks and Mudd, 2019). Lastly, the extent and details are unknown regarding the diagenetic process that, along with the primary sedimentological process, contributed to critical mineral enrichment of the deposit.

Additional research is needed to (1) verify the Ti phases in the ore, including the presence of an ilmenite-hematite solid solution mineral and the relative abundance of ilmenite, anatase leucoxene, and other phases; (2) characterize the timing and extent of the alteration process that may have enhanced enrichment in Ti and REEs; (3) determine how the concentration of critical minerals by sedimentological process and later diagenesis at Richards Gap compares to the processes that occurred at other Cretaceous heavy-mineral sand deposits in Wyoming; and (4) assess the role of heavy-mineral provenance in variations of ore grade among heavy-mineral sand deposits throughout Wyoming and elsewhere in the Rocky Mountain region.

Future work by the WSGS will investigate the critical mineral potential of several other heavy-mineral sand deposits in the Rock Spring Uplift area.

REFERENCES

Bingler, E.C., 1963, Niobium-bearing Sanostee heavy mineral deposit, San Juan Basin, northwestern New Mexico: New Mexico Bureau of Mines and Mineral Resources Circular 68, 63 p.

Dow, V.T., and Batty, J.V., 1961, Reconnaissance of titaniferous sandstone deposits in Utah, Wyoming, New Mexico, and Colorado: U.S. Bureau of Mines Report of Investigations 5860, 52 p.

Fleischer, Michael, Murata, K.J., Fletcher, J.D., and Narten, P.F., 1952, Geochemical association of niobium (columbium) and titanium and its geological and economic significance: U.S. Geological Survey Circular 225, 13 p.

Force, E.R., 2000, Titanium mineral resource of the western U.S.—An update: U.S. Geological Survey Open-File Report 00-442, 37 p.

Force, E.R., Butler, R.F., Reynolds, R.L., and Houston, R.S., 2001, Magnetic ilmenite-hematite detritus in Mesozoic–Tertiary placer and sandstone-hosted uranium deposits of the Rocky Mountains: Economic Geology, v. 96, p. 1,445–1,453.

Fortier, S.M., Nassar, N.T., Lederer, G.W., Brainard, Jamie, Gambogi, Joseph, and McCullough, E.A., 2018, Draft critical mineral list—Summary of methodology and background information—U.S. Geological Survey technical input document in response to secretarial order no. 3359: U.S. Geological Survey Open-File Report 2018-1021, 15 p.

Graybeal, F.T., and Vikre, P.G., 2010, A review of silver-rich mineral deposits and their metallogeny, *in* Goldfarb, R.J., Marsh, E.E., and Monecke, Thomas, eds., The challenge of finding new mineral resources—Global, metallogeny, innovative exploration, and new discoveries: Special Publications of the Society of Economic Geologists, v. 15, p. 85–117.

Hansen, W.R., 1957, Geology of the Clay Basin quadrangle, Utah: U.S. Geological Survey Geologic Quadrangle Map GQ-101, scale 1:24,000.

Hausel, W.D., 1990, Strategic mineral resources in Wyoming—Titanium: Geological Survey of Wyoming [Wyoming State Geological Survey] Open File Report 90-7, 18 p.

Hou, Baohong, Keeling, John, and Van Gosen, B.S., 2017, Geological and exploration models of beach placer deposits, integrated from case-studies of southern Australia: Ore Geology Reviews, v. 80, p. 437–459.

Houston, R.S., and Murphy, J.F., 1962, Titaniferous black sandstone deposits of Wyoming: Geological Survey of Wyoming [Wyoming State Geological Survey] Bulletin 49, 120 p., 7 pls.

Houston, R.S., and Murphy, J.F., 1965, Age and distribution of sedimentary zircon as a guide to provenance: U.S. Geological Survey Professional Paper 525-D, p. D22–D26.

Houston, R.S., and Murphy, J.F., 1970, Fossil beach placers in sandstones of Late Cretaceous age in Wyoming and other Rocky Mountains states: Wyoming Geological Association 22nd annual field conference guidebook, p. 241–249.

Houston, R.S., and Murphy, J.F., 1977, Depositional environment of Upper Cretaceous black sandstones of the Western Interior: U.S. Geological Survey Professional Paper 994-A, 29 p.

Jones, J.V. III, Piatak, N.M., and Bedinger, G.M., 2017, Zirconium and hafnium, *in* Schulz, K.J., DeYoung, J.H. Jr., Seal, R.R. II, and Bradley, D.C., eds., Critical mineral resources of the United States—Economic and environmental geology and prospects for future supply: U.S. Geological Survey Professional Paper 1802-V, 26 p.

Kehoe, K.S., Gay, G.W., and Lichtner, D.T., 2021, Preliminary geologic map of the Richards Gap quadrangle, Sweetwater County, Wyoming: Wyoming State Geological Survey Open File Report 2021-2, 12 p., scale 1:24,000

Kelley, K.D., Scott, Clint, Polyak, D.E., and Kimball, B.E., 2017, Vanadium, *in* Schulz, K.J., DeYoung, J.H. Jr., Seal, R.R. II, and Bradley, D.C., eds., Critical mineral resources of the United States—Economic and environmental geology and prospects for future supply: U.S. Geological Survey Professional Paper 1802-U, 36 p.

King, J.K., 1991, Rare earth elements and yttrium in Wyoming: Wyoming State Geological Survey Industrial Minerals Report 91-3, 125 p. (Supersedes Geological Survey of Wyoming Open File Report 87-8; Revised by R.E. Harris 2002.)

King, J.K., and Harris, R.E., 1987, Rare earth elements and yttrium in Wyoming: Geological Survey of Wyoming [Wyoming State Geological Survey] Open File Report 87-8, 43 p.

Madsen, Mary, 1978, A statistical analysis of heavy mineral variations in Upper Cretaceous black sandstone deposits of the Rocky Mountain states: Laramie, University of Wyoming, M.S. thesis, 139 p.

Minor, K.P., Steel, R.J., and Olariu, Cornel, 2021, Tectonic and eustatic control of Mesaverde Group (Campanian–Maastrichtian) architecture, Wyoming-Utah-Colorado region, USA: Geological Society of America Bulletin, 27 p., https://doi.org/10.1130/B36032.1.

Murphy, J.F., and Houston, R.S., 1955, Titanium-bearing black sand deposits of Wyoming: Wyoming Geological Association 10th annual field conference guidebook, p. 190–196.

Perks, Cameron, and Mudd, Gavin, 2019, Titanium, zirconium resources and production—A state of the art literature review: Ore Geology Reviews, v. 107, p. 629–646.

Roehler, H.W., 1989, Origin and distribution of six heavy-mineral placer deposits in coastal-marine sandstones in the Upper Cretaceous McCourt Sandstone Tongue of the Rock Springs Formation, southwest Wyoming: U.S. Geological Survey Bulletin 1867, 34 p., 1 pl.

Schuiling, R.D., and Feenstra, Anne, 1980, Geochemical behaviour of vanadium in iron-titanium oxides: Chemical Geology, v. 30, no. 1–2, p. 143–150.

Schulz, K.J., DeYoung, J.H. Jr., Seal, R.R. II, and Bradley, D.C., 2017a, Critical mineral resources of the United States—An introduction, *in* Schulz, K.J., DeYoung, J.H. Jr., Seal, R.R. II, and Bradley, D.C., eds., Critical mineral resources of the United States—Economic and environmental geology and prospects for future supply: U.S. Geological Survey Professional Paper 1802-A, 14 p.

Schulz, K.J., Piatak, N.M., and Papp, J.F., 2017b, Niobium and tantalum, *in* Schulz, K.J., DeYoung, J.H. Jr., Seal, R.R. II, and Bradley, D.C., eds., Critical mineral resources of the United States—Economic and environmental geology and prospects for future supply: U.S. Geological Survey Professional Paper 1802-M, 34 p.

Sutherland, W.M., and Cola, E.C., 2016, A comprehensive report on rare earth elements in Wyoming: Wyoming State Geological Survey Report of Investigations 71, 137 p.

Taylor, S.R., and McLennan, S.M., 1985, The continental crust—Its composition and evolution: Blackwell, Oxford, England, 312 p.

U.S. Geological Survey, 2006, FGDC Digital Cartographic Standard for Geologic Map Symbolization (PostScript Implementation): U.S. Geological Survey Techniques and Methods 11-A2, 261 p., 2 pls.

U.S. Nuclear Regulatory Commission, 2021, Part 40—Domestic licensing of source material, in Title 10—Energy: U.S. Federal Register Code of Federal Regulations, p. 780–840.

Van Gosen, B.S., and Ellefsen, K.J., 2018, Titanium mineral resources in heavy-mineral sands in the Atlantic Coastal Plain of the southeastern United States: U.S. Geological Survey Scientific Investigations Report 2018–5045, 32 p.

Van Gosen, B.S., Fey, D.L., Shah, A.K., Verplanck, P.L., and Hoefen, T.M., 2014, Deposit model for heavy-mineral sands in coastal environments: U.S. Geological Survey Scientific Investigations Report 2010-5070-L, 51 p.

Van Gosen, B.S., Verplanck, P.L., and Emsbo, Poul, 2019, Rare earth element mineral deposits in the United States: U.S. Geological Survey Circular 1454, 16 p.

Van Gosen, B.S., Verplanck, P.L., Seal, R.R. II, Long, K.R., and Gambogi, Joseph, 2017, Rare-earth elements, *in* Schulz, K.J., DeYoung, J.H. Jr., Seal, R.R. II, and Bradley, D.C., eds., Critical mineral resources of the United States—Economic and environmental geology and prospects for future supply: U.S. Geological Survey Professional Paper 1802-O, 31 p.

Woodruff, L.G., Bedinger, G.M., and Piatak, N.M., 2017, Titanium, *in* Schulz, K.J., DeYoung, J.H. Jr., Seal, R.R. II, and Bradley, D.C., eds., Critical mineral resources of the United States—Economic and environmental geology and prospects for future supply: U.S. Geological Survey Professional Paper 1802-T, 23 p.

Appendices

Geochemical data in the appendices of the report for the WSGS bedrock geologic map of the Richards Gap 7.5' quadrangle are reproduced and reformatted here, with an emphasis on analyses of the heavy-mineral sand deposit sampled during mapping (Kehoe and others, 2021).

Appendix 1. Sample descriptions and locations

Table A1–1. Sample name, location, and brief description for rock samples from the Richards Gap quadrangle submitted to AGAT Laboratories for elemental geochemistry. Geochemical results are reported in appendices 2 through 5.

Sample name	Map label	Latitude	Longitude	Description
RG-DL-20200721-01	RG01	41.00350	-109.21496	Salt-and-pepper sandstone at base of Gottsche Tongue
RG-DL-20200721-04	RG02	41.00305	-109.21771	Salt-and-pepper sandstone at base of Gottsche Tongue
RG-DL-20200721-05	RG03	41.00307	-109.21827	Maroon sandstone near eastern extent of HMS deposit, 0.3–0.6 m thick
RG-DL-20200721-06	RG04	41.00320	-109.21863	Maroon sandstone near eastern extent of HMS deposit, greater than 0.3 m thick (upper contact not observed)
RG-DL-20200721-07	RG05	41.00369	-109.21977	Maroon-weathering, salt-and-pepper sandstone at base of Gottsche Tongue
RG-DL-20200721-08	RG06	41.00369	-109.21977	Maroon-weathering, salt-and-pepper sandstone 1.5 m above base of Gottsche Tongue
RG-DL-20200721-09	RG07	41.00376	-109.21998	Salt-and-pepper sandstone at base of Gottsche Tongue
RG-DL-20200721-010	RG08	41.00376	-109.21997	Salt-and-pepper sandstone 1.5 m above base of Gottsche Tongue
RG-DL-20200721-011	RG09	41.00438	-109.22030	Salt-and-pepper sandstone 1.5 m above base of Gottsche Tongue
RG-DL-20200722-014	RG10	41.00623	-109.22304	Maroon sandstone lens near western extent of HMS deposit, 0.1 m thick
RG-DL-20200722-015	RG11	41.00614	-109.22278	Maroon sandstone at western extent of main HMS deposit, 0.5 m thick
RG-DL-20200722-016	RG12	41.00606	-109.22271	Maroon sandstone at base of west part of 2-m-thick HMS deposit
RG-DL-20200722-017	RG13	41.00606	-109.22271	Maroon sandstone 1 m from base of west part of 2-m-thick HMS deposit
RG-DL-20200722-018	RG14	41.00606	-109.22271	Maroon sandstone at top of west part of 2-m-thick HMS deposit, west end
RG-DL-20200722-020	RG15	41.00593	-109.22255	Maroon sandstone 1 m from base of east part of 2-m-thick HMS deposit
RG-DL-20200722-021	RG16	41.00593	-109.22255	Maroon sandstone at top of east part of 2-m-thick HMS deposit
RG-DL-20200722-022	RG17	41.00582	-109.22252	Maroon sandstone at base of 1-m-thick HMS deposit, east of maximum thickness
RG-DL-20200722-023	RG18	41.00582	-109.22252	Maroon sandstone at top of 1-m-thick HMS deposit, east of maximum thickness
RG-DL-20200722-024	RG19	41.00552	-109.22264	Maroon sandstone from middle of HMS deposit near eastern extent, 0.5 m thick
RG-DL-20200722-025	RG20	41.00454	-109.22144	Maroon sandstone from easternmost extent of HMS deposit, 0.5 m thick
RG-DL-20200722-026	RG21	41.00470	-109.22194	Maroon sandstone from eastern finger of HMS deposit, 0.3 m thick
RG-DL-20200722-027	RG22	41.00514	-109.22246	Maroon sandstone from eastern finger of HMS deposit, thickness pinches and swells, 0.1–0.6 m thick

Table A2–1. Samples from the Richards Gap quadrangle submitted to AGAT Laboratories for major element oxide geochemistry. Analytical method is AGAT 201-676, preparation by lithium borate fusion and analysis by X-ray fluorescense (XRF). Significant digits as reported from AGAT Laboratories, RDL: reported detection limit.

Sample name	Map label	Analyte															Total oxides
		Al_2O_3 (%)	BaO (%)	CaO (%)	Cr_2O_3 (%)	Fe_2O_3 (%)	K_2O (%)	MgO (%)	MnO (%)	Na_2O (%)	P_2O_5 (%)	SiO_2 (%)	TiO_2 (%)	SrO (%)	V_2O_5 (%)	LOI (%)	(%)
RG-DL-20200721-01	RG01	1.15	0.07	0.28	0.03	0.50	0.17	0.38	<0.01	0.11	0.04	96.20	0.04	<0.01	<0.01	1.24	100.00
RG-DL-20200721-04	RG02	1.78	0.11	0.47	0.04	0.84	0.18	0.17	<0.01	0.07	0.07	94.50	0.08	<0.01	<0.01	1.36	99.70
RG-DL-20200721-05	RG03	2.39	0.09	0.57	0.05	30.40	0.24	0.66	0.48	0.08	0.21	19.20	39.00	0.02	0.19	3.33	96.90
RG-DL-20200721-06	RG04	4.27	0.04	0.28	0.02	20.70	0.82	0.34	0.27	0.12	0.06	67.10	2.18	<0.01	0.02	4.02	100.00
RG-DL-20200721-07	RG05	1.03	0.11	0.31	0.04	0.58	0.14	0.12	0.01	0.08	0.07	95.80	0.11	<0.01	<0.01	0.68	99.10
RG-DL-20200721-08	RG06	0.96	0.07	0.22	0.04	0.57	0.13	0.13	<0.01	0.04	0.04	96.30	0.14	<0.01	<0.01	1.01	99.70
RG-DL-20200721-09	RG07	1.07	0.09	0.14	0.05	0.44	0.15	0.09	<0.01	0.04	0.05	96.90	0.07	<0.01	<0.01	0.60	99.70
RG-DL-20200721-010	RG08	1.35	0.10	0.24	0.04	0.44	0.16	0.15	<0.01	0.04	0.07	96.00	0.09	<0.01	<0.01	1.04	99.70
RG-DL-20200721-011	RG09	1.16	0.07	0.22	0.05	0.52	0.16	0.09	<0.01	0.06	0.04	96.60	0.08	<0.01	<0.01	0.83	99.90
RG-DL-20200722-014	RG10	2.03	0.01	0.08	<0.01	68.00	0.20	0.09	0.98	0.02	0.19	16.80	0.22	<0.01	<0.01	11.50	100.00
RG-DL-20200722-015	RG11	4.47	0.07	1.26	0.02	16.10	0.83	0.59	0.24	0.08	0.04	68.40	2.45	<0.01	0.01	5.27	99.80
RG-DL-20200722-016	RG12	5.75	0.04	0.29	0.03	8.51	0.87	0.40	0.26	0.11	0.12	73.60	6.07	<0.01	0.03	3.33	99.40
RG-DL-20200722-017	RG13	3.89	0.07	0.13	0.03	18.60	0.54	0.23	0.45	0.05	0.12	45.40	24.00	<0.01	0.11	4.34	98.00
RG-DL-20200722-018	RG14	3.93	0.07	1.19	0.03	16.40	0.58	0.68	0.39	0.04	0.11	48.10	21.00	<0.01	0.09	5.58	98.20
RG-DL-20200722-020	RG15	1.63	0.05	2.88	0.05	43.10	0.07	2.16	0.76	<0.01	0.17	5.03	37.60	0.01	0.22	4.66	98.40
RG-DL-20200722-021	RG16	3.44	0.06	2.75	0.03	22.80	0.50	1.19	0.44	0.06	0.11	42.90	16.80	<0.01	0.09	7.64	98.80
RG-DL-20200722-022	RG17	4.06	0.09	0.66	0.05	27.00	0.32	1.05	0.67	0.16	0.26	20.40	35.60	0.02	0.19	6.65	97.20
RG-DL-20200722-023	RG18	2.05	0.08	0.47	0.04	42.60	0.11	1.19	0.66	0.01	0.17	7.30	40.40	<0.01	0.20	2.38	97.70
RG-DL-20200722-024	RG19	1.76	0.08	3.45	0.04	39.60	0.11	1.22	0.71	0.02	0.19	7.29	39.40	0.03	0.19	4.20	98.30
RG-DL-20200722-025	RG20	5.52	0.04	0.10	0.02	11.90	1.25	0.19	0.05	0.20	0.08	76.00	1.34	<0.01	0.01	3.25	100.00
RG-DL-20200722-026	RG21	4.39	0.09	0.62	0.03	17.10	0.79	0.34	0.16	0.15	0.12	57.80	14.50	<0.01	0.07	4.17	100.00
RG-DL-20200722-027	RG22	4.39	0.07	0.61	0.02	17.30	0.74	0.50	0.15	0.15	0.11	57.10	15.10	0.01	0.07	2.83	99.20
	RDL:	0.01	0.01	0.01	0.01	0.01	0.01	0.01	0.01	0.01	0.01	0.01	0.01	0.01	0.01	0.01	0.01

Appendix 3. Trace element geochemistry, sodium peroxide fusion

Table A3–1. Samples from the Richards Gap quadrangle submitted to AGAT Laboratories for trace element geochemistry. Results reported as parts per million (ppm) or as weight percent (%). Analytical method is AGAT 201-378, preparation by sodium peroxide fusion and analysis by inductively coupled plasma mass spectrometry (ICP-MS) and ICP optical emission spectrometry (ICP-OES). Significant digits as reported from AGAT Laboratories, RDL: reported detection limit.

Sample name	Map label	Analyte									
		Ag (ppm)	Al (%)	As (ppm)	B (ppm)	Ba (ppm)	Be (ppm)	Bi (ppm)	Ca (%)	Cd (ppm)	Ce (ppm)
RG-DL-20200721-01	RG01	<1	0.62	55	24	586	<5	<0.1	0.2	<0.2	22.8
RG-DL-20200721-04	RG02	1	0.97	48	27	949	<5	<0.1	0.35	<0.2	42
RG-DL-20200721-05	RG03	7	1.34	35	<20	784	<5	0.3	0.48	<0.2	1,920
RG-DL-20200721-06	RG04	<1	2.34	26	<20	337	<5	<0.1	0.22	<0.2	175
RG-DL-20200721-07	RG05	1	0.56	26	23	980	<5	<0.1	0.22	<0.2	40.1
RG-DL-20200721-08	RG06	2	0.52	21	24	599	<5	<0.1	0.18	<0.2	37.5
RG-DL-20200721-09	RG07	1	0.59	17	29	692	<5	<0.1	0.12	<0.2	34.8
RG-DL-20200721-010	RG08	1	0.72	15	28	1,010	<5	<0.1	0.19	<0.2	46.3
RG-DL-20200721-011	RG09	<1	0.62	12	23	708	<5	<0.1	0.16	<0.2	31.7
RG-DL-20200722-014	RG10	<1	1.07	11	<20	128	<5	<0.1	0.11	<0.2	45.5
RG-DL-20200722-015	RG11	1	2.41	11	35	690	<5	<0.1	0.9	<0.2	328
RG-DL-20200722-016	RG12	2	3.08	12	84	331	<5	0.2	0.23	<0.2	1,200
RG-DL-20200722-017	RG13	5	2.22	15	<20	593	<5	0.3	0.15	0.5	1,560
RG-DL-20200722-018	RG14	5	2.16	14	<20	500	<5	0.3	0.87	<0.2	1,230
RG-DL-20200722-020	RG15	8	0.92	12	<20	368	<5	0.3	2.1	<0.2	1,410
RG-DL-20200722-021	RG16	4	1.98	13	<20	482	<5	0.2	2.05	<0.2	799
RG-DL-20200722-022	RG17	8	2.25	22	<20	833	<5	0.5	0.54	0.3	5,000
RG-DL-20200722-023	RG18	7	1.1	53	<20	726	<5	0.4	0.35	0.4	1,310
RG-DL-20200722-024	RG19	7	0.96	35	<20	746	<5	0.3	2.4	0.2	1,590
RG-DL-20200722-025	RG20	1	2.99	37	23	375	<5	<0.1	0.12	<0.2	76
RG-DL-20200722-026	RG21	3	2.37	28	<20	785	<5	0.2	0.46	<0.2	461
RG-DL-20200722-027	RG22	3	2.41	23	20	706	<5	0.2	0.49	0.3	471
	RDL:	1	0.01	5	20	0.5	5	0.1	0.05	0.2	0.1

Table A3-1. continued

Sample name	Map label	Analyte									
		Co (ppm)	Cr (%)	Cs (ppm)	Cu (ppm)	Dy (ppm)	Er (ppm)	Eu (ppm)	Fe (%)	Ga (ppm)	Gd (ppm)
RG-DL-20200721-01	RG01	0.8	0.023	0.3	13	0.88	0.4	0.21	0.39	1.73	1.38
RG-DL-20200721-04	RG02	2.7	0.027	0.5	27	1.54	0.56	0.54	0.65	2.5	2.71
RG-DL-20200721-05	RG03	31.3	0.037	0.2	16	44.3	31.6	9.35	23	17.5	66
RG-DL-20200721-06	RG04	5.9	0.012	0.9	7	5.08	3.13	0.99	15.9	5.83	6.75
RG-DL-20200721-07	RG05	1.2	0.03	0.3	12	1.28	0.56	0.43	0.44	1.49	2.35
RG-DL-20200721-08	RG06	1.5	0.033	0.3	20	1.11	0.54	0.33	0.45	1.39	1.95
RG-DL-20200721-09	RG07	1.1	0.033	0.4	<5	1.12	0.5	0.4	0.34	1.45	2.07
RG-DL-20200721-010	RG08	1.9	0.03	0.4	30	1.7	0.75	0.59	0.34	1.79	2.92
RG-DL-20200721-011	RG09	1.1	0.039	0.3	7	1.38	0.64	0.37	0.39	1.6	1.99
RG-DL-20200722-014	RG10	17.6	0.006	0.7	8	2.79	1.64	0.46	48.2	2.57	3.06
RG-DL-20200722-015	RG11	13.4	0.018	1	5	11.2	6.85	2.12	12.3	7.15	15
RG-DL-20200722-016	RG12	19.7	0.025	0.9	7	24.3	13.3	5.58	6.49	14.9	40.2
RG-DL-20200722-017	RG13	37.2	0.027	0.5	11	42.1	26.6	8.76	14.9	17.3	65.8
RG-DL-20200722-018	RG14	43.3	0.026	0.7	11	33.2	22.6	7.06	12.6	16.9	50.5
RG-DL-20200722-020	RG15	49.2	0.033	<0.1	14	39	27.5	7.43	32.4	21.7	56.6
RG-DL-20200722-021	RG16	35.2	0.024	0.5	9	25.6	16.9	4.9	17.6	13.4	34.5
RG-DL-20200722-022	RG17	67.7	0.042	0.2	16	66.7	37.4	15.4	21.3	33.8	122
RG-DL-20200722-023	RG18	70.4	0.031	<0.1	14	37.4	26.4	6.69	30.8	19.7	49.8
RG-DL-20200722-024	RG19	51.3	0.031	<0.1	12	34.2	23.9	6.8	28.9	17.2	51.8
RG-DL-20200722-025	RG20	19.7	0.019	1.8	8	4.33	2.91	0.76	9.19	6.77	4.81
RG-DL-20200722-026	RG21	36.4	0.019	0.7	9	13.5	8.91	2.54	13.1	9.08	17.4
RG-DL-20200722-027	RG22	15.2	0.019	0.7	8	13.5	9.17	2.68	13.4	9.27	17.3
	RDL:	0.5	0.005	0.1	5	0.05	0.05	0.05	0.01	0.01	0.05

Table A3-1. continued

Sample name	Map label	Analyte									
		Ge (ppm)	Hf (ppm)	Ho (ppm)	In (ppm)	K (%)	La (ppm)	Li (ppm)	Lu (ppm)	Mg (%)	Mn (ppm)
RG-DL-20200721-01	RG01	<1	1	0.16	<0.2	0.15	14.6	<10	0.06	0.21	20
RG-DL-20200721-04	RG02	1	2	0.23	<0.2	0.15	27.9	<10	0.08	0.1	26
RG-DL-20200721-05	RG03	3	672	9.66	0.5	0.23	1,080	<10	7.22	0.41	4,250
RG-DL-20200721-06	RG04	3	24	1	<0.2	0.72	97.5	<10	0.55	0.21	2,260
RG-DL-20200721-07	RG05	1	2	0.22	<0.2	0.11	25.8	<10	0.07	0.07	37
RG-DL-20200721-08	RG06	1	2	0.18	<0.2	0.11	23.9	<10	0.07	0.08	46
RG-DL-20200721-09	RG07	1	1	0.21	<0.2	0.13	22.7	<10	0.06	0.05	24
RG-DL-20200721-010	RG08	3	4	0.26	<0.2	0.14	30.4	<10	0.08	0.09	43
RG-DL-20200721-011	RG09	<1	2	0.23	<0.2	0.13	20.2	<10	0.08	0.06	31
RG-DL-20200722-014	RG10	5	4	0.56	<0.2	0.19	21.4	<10	0.26	0.03	7,470
RG-DL-20200722-015	RG11	1	43	2.1	<0.2	0.68	205	11	1.08	0.36	1,990
RG-DL-20200722-016	RG12	2	96	4.62	<0.2	0.74	680	10	2.11	0.23	2,190
RG-DL-20200722-017	RG13	3	422	8.22	0.3	0.48	1,160	12	5.4	0.14	4,060
RG-DL-20200722-018	RG14	3	438	6.88	0.3	0.5	743	10	5.04	0.43	3,380
RG-DL-20200722-020	RG15	2	606	8.16	0.5	0.08	889	<10	6.39	1.36	6,630
RG-DL-20200722-021	RG16	1	335	5.15	0.2	0.46	441	<10	3.72	0.76	3,880
RG-DL-20200722-022	RG17	5	369	12.7	0.5	0.29	2,830	16	6.64	0.69	6,300
RG-DL-20200722-023	RG18	2	561	7.97	0.5	0.08	831	<10	6.22	0.71	5,610
RG-DL-20200722-024	RG19	2	481	7.3	0.5	0.09	986	<10	5.57	0.74	6,210
RG-DL-20200722-025	RG20	1	18	0.93	<0.2	1.03	43.7	<10	0.45	0.11	441
RG-DL-20200722-026	RG21	3	109	2.9	0.2	0.66	266	<10	1.67	0.21	1,240
RG-DL-20200722-027	RG22	2	121	2.9	0.2	0.63	255	<10	1.82	0.32	1,230
	RDL:	1	1	0.05	0.2	0.05	0.1	10	0.05	0.01	10

Table A3-1. continued

Sample name	Map label	Analyte									
		Mo (ppm)	Nb (ppm)	Nd (ppm)	Ni (ppm)	P (%)	Pb (ppm)	Pr (ppm)	Rb (ppm)	S (%)	Sb (ppm)
RG-DL-20200721-01	RG01	15	<1	9.4	18	0.01	12	2.72	5.5	0.06	0.2
RG-DL-20200721-04	RG02	18	2	17.9	15	0.03	23	5.24	7.9	0.27	0.3
RG-DL-20200721-05	RG03	6	503	647	11	0.09	62	206	8.6	0.03	6.4
RG-DL-20200721-06	RG04	6	30	58.2	14	0.03	9	18	28.4	0.01	0.7
RG-DL-20200721-07	RG05	19	2	16.1	19	0.03	15	4.66	5.8	0.06	0.1
RG-DL-20200721-08	RG06	23	3	14.1	17	0.01	12	4.24	5.1	0.06	0.1
RG-DL-20200721-09	RG07	20	2	14.3	16	0.02	16	4	5.9	0.05	<0.1
RG-DL-20200721-010	RG08	21	2	19.3	17	0.03	20	5.55	6.6	0.07	0.1
RG-DL-20200721-011	RG09	25	2	12.9	20	0.02	15	3.77	6.7	0.06	<0.1
RG-DL-20200722-014	RG10	4	5	18.7	<5	0.09	5	5.21	10.1	0.59	0.4
RG-DL-20200722-015	RG11	9	41	117	16	0.02	11	35.9	28.3	0.08	1.1
RG-DL-20200722-016	RG12	11	130	374	25	0.06	24	118	32.9	0.01	3.4
RG-DL-20200722-017	RG13	6	305	587	28	0.06	36	187	20.1	0.05	4.2
RG-DL-20200722-018	RG14	6	305	437	23	0.05	36	137	21.8	0.12	4.7
RG-DL-20200722-020	RG15	4	448	513	11	0.07	42	161	2.8	0.05	4
RG-DL-20200722-021	RG16	6	220	273	13	0.06	28	84.4	17	0.08	2.6
RG-DL-20200722-022	RG17	6	496	1,560	28	0.12	58	416	10.8	0.1	9.7
RG-DL-20200722-023	RG18	4	458	469	13	0.07	48	143	3.7	0.04	4.7
RG-DL-20200722-024	RG19	4	425	527	8	0.07	40	166	4.1	0.06	4.2
RG-DL-20200722-025	RG20	10	20	28.7	30	0.04	9	8.3	42.7	0.07	0.8
RG-DL-20200722-026	RG21	9	156	146	23	0.05	17	46.5	26.6	0.07	2.6
RG-DL-20200722-027	RG22	9	162	154	13	0.05	17	48.1	25.5	0.02	2.7
	RDL:	2	1	0.1	5	0.01	5	0.05	0.2	0.01	0.1

Table A3-1. continued

Sample name	Map label	Analyte									
		Sc (ppm)	Si (%)	Sm (ppm)	Sn (ppm)	Sr (ppm)	Ta (ppm)	Tb (ppm)	Th (ppm)	Ti (%)	Tl (ppm)
RG-DL-20200721-01	RG01	<5	43.8	1.6	<1	56.3	<0.5	0.22	0.9	0.03	<0.5
RG-DL-20200721-04	RG02	<5	45.6	3	3	100	<0.5	0.35	1.5	0.04	0.6
RG-DL-20200721-05	RG03	92	9.21	83.9	32	171	33	9.4	279	22.9	<0.5
RG-DL-20200721-06	RG04	9	33.4	8.2	1	44	2.1	1.05	27.8	1.24	<0.5
RG-DL-20200721-07	RG05	<5	45.1	2.6	<1	79.3	<0.5	0.29	2	0.07	<0.5
RG-DL-20200721-08	RG06	<5	46.7	2.3	2	65.8	<0.5	0.26	2.5	0.09	<0.5
RG-DL-20200721-09	RG07	<5	45.5	2.2	<1	73.8	<0.5	0.29	1.2	0.04	<0.5
RG-DL-20200721-010	RG08	<5	44.7	3.3	4	105	<0.5	0.37	1.6	0.05	<0.5
RG-DL-20200721-011	RG09	<5	44.7	2.1	<1	70	<0.5	0.3	1.4	0.04	<0.5
RG-DL-20200722-014	RG10	<5	8.18	3.1	<1	17.3	<0.5	0.51	3.4	0.12	<0.5
RG-DL-20200722-015	RG11	15	33.3	17.2	2	54.8	3.1	2.23	34.7	1.39	<0.5
RG-DL-20200722-016	RG12	22	35.6	49.9	7	79	10.9	5.7	120	3.5	<0.5
RG-DL-20200722-017	RG13	66	23.1	75.7	17	89.9	21.3	8.99	178	15.7	<0.5
RG-DL-20200722-018	RG14	57	23.4	61.1	17	98.9	20.6	7.26	182	13.8	<0.5
RG-DL-20200722-020	RG15	100	2.43	70.4	27	120	27.7	8.2	211	21.9	<0.5
RG-DL-20200722-021	RG16	50	21.9	41.3	11	91.4	14.8	5.15	106	9.36	<0.5
RG-DL-20200722-022	RG17	102	10.5	156	23	221	34.4	16.1	450	21.2	<0.5
RG-DL-20200722-023	RG18	101	3.38	61.8	24	114	31.4	7.17	196	22.5	0.9
RG-DL-20200722-024	RG19	104	3.49	66.1	20	206	26.9	7.21	209	22.2	<0.5
RG-DL-20200722-025	RG20	9	37.6	4.7	2	51.3	1.4	0.8	14.9	0.75	<0.5
RG-DL-20200722-026	RG21	40	28.4	20.6	11	124	10.9	2.56	86.9	8.26	<0.5
RG-DL-20200722-027	RG22	40	28.8	22.5	9	133	11.2	2.74	109	8.5	<0.5
	RDL:	5	0.01	0.1	1	0.1	0.5	0.05	0.1	0.01	0.5

Table A3-1. continued

Sample name	Map label	Analyte							
		Tm (ppm)	U (ppm)	V (ppm)	W (ppm)	Y (ppm)	Yb (ppm)	Zn (ppm)	Zr (ppm)
RG-DL-20200721-01	RG01	0.05	0.46	15	<1	4.7	0.3	<5	36
RG-DL-20200721-04	RG02	0.08	0.66	17	<1	6.8	0.5	6	54
RG-DL-20200721-05	RG03	5.43	54.6	1,070	17	278	40.6	201	30,300
RG-DL-20200721-06	RG04	0.48	5.32	90	1	25.1	3.4	77	987
RG-DL-20200721-07	RG05	0.07	0.65	15	<1	5.5	0.4	9	87
RG-DL-20200721-08	RG06	0.06	0.65	14	<1	5	0.5	<5	91
RG-DL-20200721-09	RG07	0.07	0.58	15	<1	5.6	0.4	6	46
RG-DL-20200721-010	RG08	0.08	0.83	18	<1	6.9	0.6	<5	179
RG-DL-20200721-011	RG09	0.09	0.64	13	<1	7.1	0.5	<5	76
RG-DL-20200722-014	RG10	0.25	0.83	12	<1	13.1	1.7	47	145
RG-DL-20200722-015	RG11	1.03	6.4	94	2	61.5	6.9	248	1,890
RG-DL-20200722-016	RG12	1.94	14.6	187	8	125	13.6	261	4,140
RG-DL-20200722-017	RG13	4.28	41.9	684	12	243	31.2	466	19,300
RG-DL-20200722-018	RG14	3.86	43.5	601	9	181	28.3	233	19,600
RG-DL-20200722-020	RG15	4.7	59	1,260	13	228	36	485	27,500
RG-DL-20200722-021	RG16	2.88	32.7	564	7	133	21.9	285	15,400
RG-DL-20200722-022	RG17	5.73	46.7	1,160	22	357	41.9	338	17,000
RG-DL-20200722-023	RG18	4.44	52.4	1,190	13	221	35.4	478	24,000
RG-DL-20200722-024	RG19	4.04	46.1	1,120	13	209	31.3	493	21,300
RG-DL-20200722-025	RG20	0.44	3.55	75	1	26.6	3	151	684
RG-DL-20200722-026	RG21	1.37	13	408	6	75.8	10.4	128	4,900
RG-DL-20200722-027	RG22	1.42	17.6	435	5	74	10.7	93	5,410
	RDL:	0.05	0.05	5	1	0.5	0.1	5	0.5

Appendix 4. Trace metals geochemistry, acid digestion

Table A4–1. Samples from the Richards Gap quadrangle submitted to AGAT Laboratories for trace element geochemistry. Units reported as parts per million (ppm) or as weight percent (%). Method is AGAT 201-070, preparation by four-acid digestion and analysis by inductively coupled plasma optical emission spectrometry (ICP-OES). Significant digits as reported from AGAT Laboratories, RDL: reported detection limit.

Sample name	Map label	Analyte									
		Ag (ppm)	Al (%)	As (ppm)	Ba (ppm)	Be (ppm)	Bi (ppm)	Ca (%)	Cd (ppm)	Ce (ppm)	Co (ppm)
RG-DL-20200721-05	RG03	<0.5	1.14	31	685	3.4	<1	0.36	0.5	1,980	17.8
RG-DL-20200721-06	RG04	<0.5	2.08	<1	300	3.5	<1	0.11	<0.5	165	1.7
RG-DL-20200721-09	RG07	<0.5	0.5	<1	653	<0.5	<1	0.09	<0.5	33	0.6
RG-DL-20200722-014	RG10	0.6	0.97	<1	117	1.8	<1	0.06	0.8	47	17
RG-DL-20200722-015	RG11	<0.5	2.18	4	668	2.9	<1	0.82	<0.5	309	9.5
RG-DL-20200722-016	RG12	<0.5	2.72	21	317	2.1	<1	0.19	0.5	1,110	13.5
RG-DL-20200722-017	RG13	<0.5	1.86	40	511	3.8	<1	0.08	1	1,450	26.6
RG-DL-20200722-018	RG14	<0.5	1.93	20	429	2.3	<1	0.77	<0.5	1,170	31.1
RG-DL-20200722-020	RG15	<0.5	0.78	19	327	2.6	<1	1.77	0.7	1,480	25.3
RG-DL-20200722-021	RG16	<0.5	1.68	5	422	2	<1	1.74	<0.5	716	23.3
RG-DL-20200722-022	RG17	<0.5	1.95	87	699	4.2	<1	0.42	1	4,090	49.4
RG-DL-20200722-023	RG18	<0.5	1	14	696	3.7	<1	0.29	0.8	1,530	44.6
RG-DL-20200722-024	RG19	<0.5	0.84	28	677	3.2	<1	2.13	0.6	1,730	34.1
RG-DL-20200722-025	RG20	<0.5	2.7	6	348	1.6	<1	0.07	<0.5	78	17.8
RG-DL-20200722-026	RG21	<0.5	2.08	1	694	2.2	<1	0.4	<0.5	457	29.4
RG-DL-20200722-027	RG22	<0.5	2.13	1	651	2.4	<1	0.4	0.6	491	9.2
	RDL:	0.5	0.01	1	1	0.5	1	0.01	0.5	1	0.5

Table A4-1. continued

Sample name	Map label	Analyte									
		Cr (ppm)	Cu (ppm)	Fe (%)	Ga (ppm)	In (ppm)	K (%)	La (ppm)	Li (ppm)	Mg (%)	Mn (ppm)
RG-DL-20200721-05	RG03	178	6.9	19.9	<5	<1	0.17	1,090	5	0.37	3,400
RG-DL-20200721-06	RG04	91.3	5.5	14.3	6	<1	0.61	92	8	0.19	2,030
RG-DL-20200721-09	RG07	123	3.7	0.31	<5	<1	0.11	21	7	0.05	25
RG-DL-20200722-014	RG10	55.8	9.4	45.6	6	<1	0.15	20	3	0.05	6,800
RG-DL-20200722-015	RG11	153	4.1	11.2	5	<1	0.61	190	9	0.33	1,810
RG-DL-20200722-016	RG12	165	2.5	5.99	<5	<1	0.64	655	10	0.21	1,930
RG-DL-20200722-017	RG13	145	4.2	12.7	<5	<1	0.39	1,090	9	0.13	3,260
RG-DL-20200722-018	RG14	134	3.6	11.4	<5	<1	0.43	681	9	0.39	2,760
RG-DL-20200722-020	RG15	203	5.1	26.7	7	<1	0.05	836	8	1.17	5,160
RG-DL-20200722-021	RG16	121	3.3	15.3	7	<1	0.37	393	7	0.67	3,110
RG-DL-20200722-022	RG17	228	6	18.3	<5	<1	0.23	2,370	13	0.57	5,030
RG-DL-20200722-023	RG18	195	3.3	27.4	<5	<1	0.07	867	8	0.63	4,640
RG-DL-20200722-024	RG19	169	4.7	24.9	<5	<1	0.08	987	7	0.64	4,950
RG-DL-20200722-025	RG20	150	5.5	8.28	6	<1	0.91	42	9	0.11	413
RG-DL-20200722-026	RG21	125	3.4	11.3	6	<1	0.57	257	6	0.2	1,060
RG-DL-20200722-027	RG22	105	3.6	11.8	<5	<1	0.55	253	8	0.29	1,080
	RDL:	0.5	0.5	0.01	5	1	0.01	2	1	0.01	1

Table A4-1. continued

Sample name	Map label	Analyte									
		Mo (ppm)	Na (%)	Ni (ppm)	P (ppm)	Pb (ppm)	Rb (ppm)	S (%)	Sb (ppm)	Sc (ppm)	Se (ppm)
RG-DL-20200721-05	RG03	<0.5	0.05	17.8	92	37	<10	0.02	<1	66	<10
RG-DL-20200721-06	RG04	4.2	0.07	8.9	207	<1	17	0.01	<1	8	<10
RG-DL-20200721-09	RG07	18.6	0.02	5.5	199	15	<10	0.05	<1	<1	<10
RG-DL-20200722-014	RG10	<0.5	0.01	17.1	733	<1	<10	0.54	5	<1	<10
RG-DL-20200722-015	RG11	8	0.06	14.1	155	4	17	0.07	<1	13	<10
RG-DL-20200722-016	RG12	1	0.07	18.4	225	17	19	0.01	<1	20	<10
RG-DL-20200722-017	RG13	<0.5	0.04	26.9	53	20	10	0.03	<1	48	<10
RG-DL-20200722-018	RG14	<0.5	0.04	21.7	74	19	11	0.07	<1	40	<10
RG-DL-20200722-020	RG15	<0.5	0.01	19.9	117	10	<10	0.02	<1	77	<10
RG-DL-20200722-021	RG16	<0.5	0.05	16.3	74	10	<10	0.02	<1	37	<10
RG-DL-20200722-022	RG17	<0.5	0.11	34.2	150	32	<10	0.06	<1	73	<10
RG-DL-20200722-023	RG18	<0.5	0.02	30.4	138	9	<10	0.04	<1	84	<10
RG-DL-20200722-024	RG19	<0.5	0.02	20.2	100	13	<10	0.02	<1	80	<10
RG-DL-20200722-025	RG20	8.4	0.14	24.5	351	2	26	0.08	<1	8	<10
RG-DL-20200722-026	RG21	<0.5	0.11	24	160	<1	15	0.05	<1	28	<10
RG-DL-20200722-027	RG22	<0.5	0.11	13.2	93	3	15	0.01	<1	31	<10
	RDL:	0.5	0.01	0.5	10	1	10	0.01	1	1	10

Table A4-1. continued

Sample name	Map label	Analyte									
		Sn (ppm)	Sr (ppm)	Ta (ppm)	Te (ppm)	Th (ppm)	Ti (%)	Tl (ppm)	U (ppm)	V (ppm)	W (ppm)
RG-DL-20200721-05	RG03	7	142	<10	16	197	1.8	<5	<5	172	<1
RG-DL-20200721-06	RG04	<5	35	<10	<10	17	0.9	<5	<5	72.1	<1
RG-DL-20200721-09	RG07	<5	64	<10	<10	<5	0.04	<5	<5	13	<1
RG-DL-20200722-014	RG10	<5	13	<10	54	<5	0.1	<5	<5	32.4	<1
RG-DL-20200722-015	RG11	<5	48	<10	<10	23	0.74	<5	<5	68.3	<1
RG-DL-20200722-016	RG12	<5	67	<10	<10	102	1.12	<5	<5	73.4	<1
RG-DL-20200722-017	RG13	5	71	<10	11	132	1.46	<5	<5	108	<1
RG-DL-20200722-018	RG14	<5	84	<10	<10	143	1.54	<5	<5	71.2	<1
RG-DL-20200722-020	RG15	6	101	<10	13	131	2.46	<5	<5	335	<1
RG-DL-20200722-021	RG16	<5	74	<10	<10	77	1.66	<5	<5	61.7	<1
RG-DL-20200722-022	RG17	7	181	<10	23	359	2	<5	<5	280	<1
RG-DL-20200722-023	RG18	8	102	<10	12	132	3.33	<5	<5	385	<1
RG-DL-20200722-024	RG19	6	178	<10	19	140	2.07	<5	<5	246	<1
RG-DL-20200722-025	RG20	<5	43	<10	<10	10	0.52	<5	<5	66.7	<1
RG-DL-20200722-026	RG21	<5	100	<10	<10	69	1.42	<5	<5	71.1	<1
RG-DL-20200722-027	RG22	<5	111	<10	<10	90	1.29	<5	<5	41.5	<1
	RDL:	5	1	10	10	5	0.01	5	5	0.5	1

Table A4-1. continued

Sample name	Map label	Analyte		
		Y (ppm)	Zn (ppm)	Zr (ppm)
RG-DL-20200721-05	RG03	114	158	811
RG-DL-20200721-06	RG04	13	70.7	109
RG-DL-20200721-09	RG07	5	4.7	13
RG-DL-20200722-014	RG10	12	35	18
RG-DL-20200722-015	RG11	44	229	93
RG-DL-20200722-016	RG12	71	236	114
RG-DL-20200722-017	RG13	133	396	311
RG-DL-20200722-018	RG14	89	206	147
RG-DL-20200722-020	RG15	105	398	750
RG-DL-20200722-021	RG16	68	249	99
RG-DL-20200722-022	RG17	203	273	750
RG-DL-20200722-023	RG18	111	437	890
RG-DL-20200722-024	RG19	101	425	691
RG-DL-20200722-025	RG20	17	148	69
RG-DL-20200722-026	RG21	37	114	67
RG-DL-20200722-027	RG22	33	77.8	52
	RDL:	1	0.5	5

Appendix 5. Au, Pt, and Pd by fire assay

Table A5–1. Samples submitted to AGAT Laboratories for Au, Pt, and Pd elemental geochemistry. Analytical method is AGAT 202-055, preparation by fire assay and analysis by inductively coupled plasma optical emission spectrometry (ICP-OES). Significant digits as reported from AGAT Laboratories, RDL: reported detection limit.

Sample name	Map label	Analyte		
		Au	Pd	Pt
		(ppm)	(ppm)	(ppm)
RG-DL-20200721-05	RG03	0.01	<0.001	0.01
RG-DL-20200721-06	RG04	0.00	<0.001	<0.005
RG-DL-20200721-09	RG07	0.00	<0.001	<0.005
RG-DL-20200722-014	RG10	0.00	<0.001	<0.005
RG-DL-20200722-015	RG11	0.00	<0.001	<0.005
RG-DL-20200722-016	RG12	0.00	<0.001	<0.005
RG-DL-20200722-017	RG13	0.00	0.00	<0.005
RG-DL-20200722-018	RG14	<0.001	<0.001	<0.005
RG-DL-20200722-020	RG15	0.01	<0.001	0.01
RG-DL-20200722-021	RG16	0.00	<0.001	<0.005
RG-DL-20200722-022	RG17	0.01	<0.001	0.01
RG-DL-20200722-023	RG18	0.00	<0.001	<0.005
RG-DL-20200722-024	RG19	<0.001	<0.001	<0.005
RG-DL-20200722-025	RG20	0.00	<0.001	<0.005
RG-DL-20200722-026	RG21	0.00	<0.001	<0.005
RG-DL-20200722-027	RG22	<0.001	<0.001	<0.005
	RDL:	0.001	0.001	0.005

Appendix 6. Photomicrographs

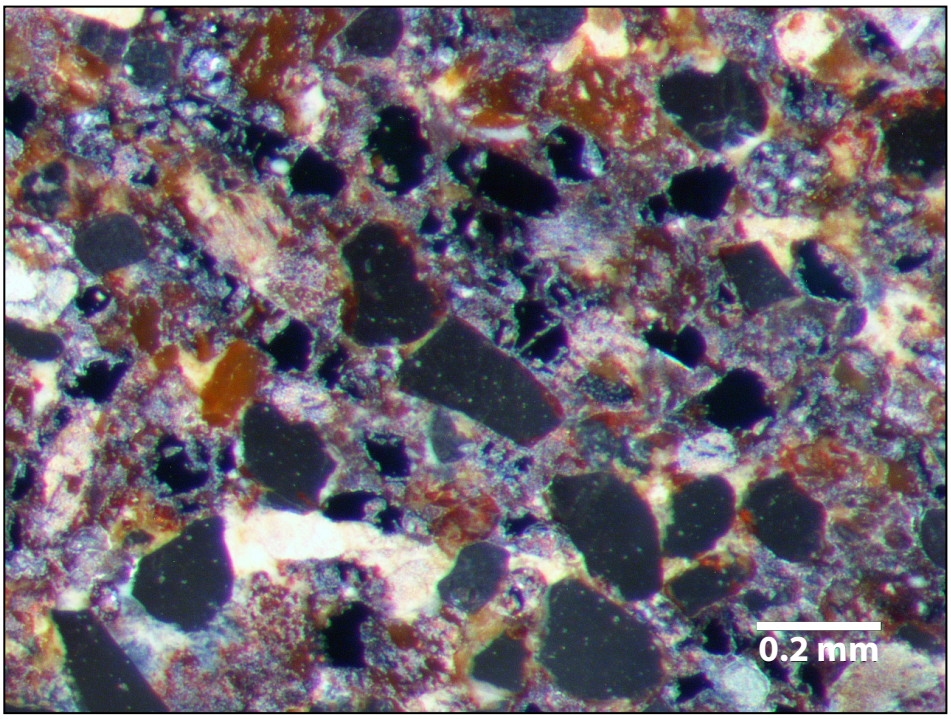

Figure A6–1. Reflected-light photomicrograph of sample RG-DL-20200721-05 (map label RG03).

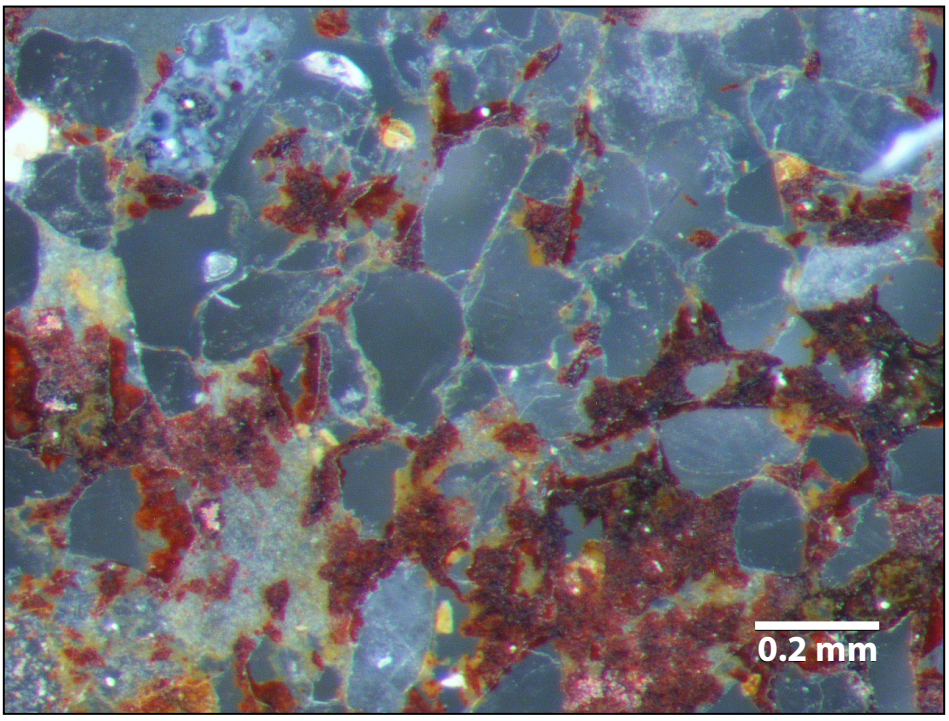

Figure A6–2. Reflected-light photomicrograph of sample RG-DL-20200721-06 (map label RG04).

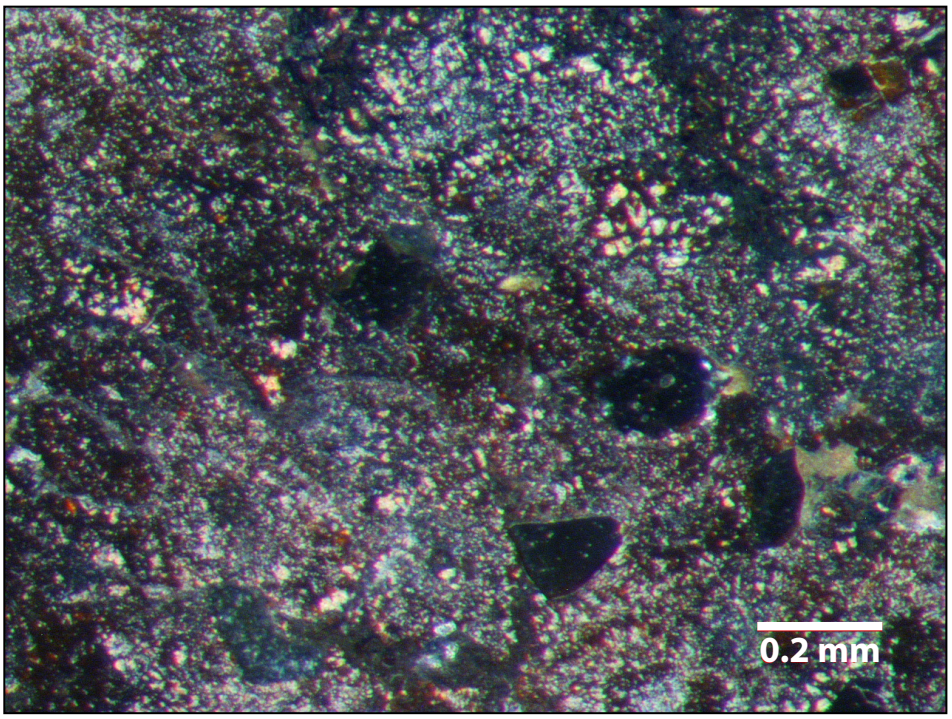

Figure A6–3. Reflected-light photomicrograph of sample RG-DL-20200722-14 (map label RG10).

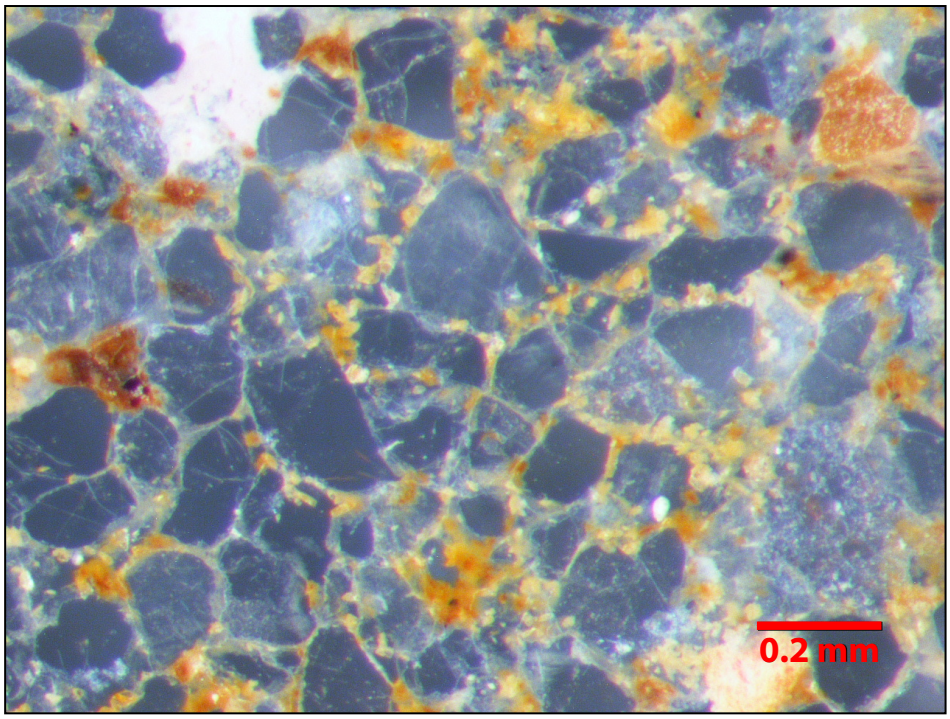

Figure A6–4. Reflected-light photomicrograph of sample RG-DL-20200722-15 (map label RG11).

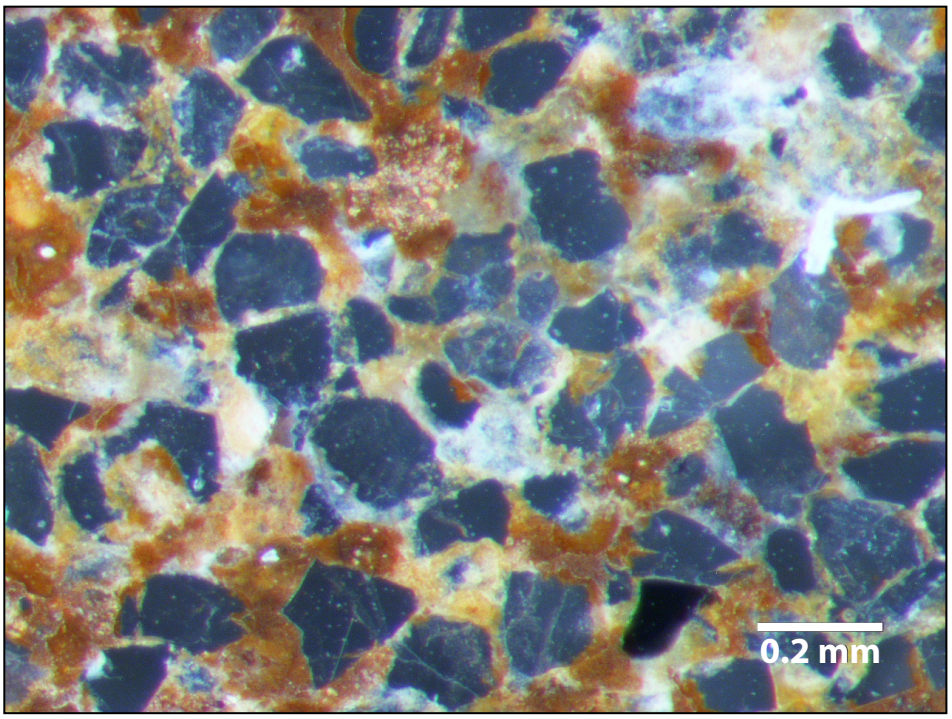

Figure A6–5. Reflected-light photomicrograph of sample RG-DL-20200722-16 (map label RG12).

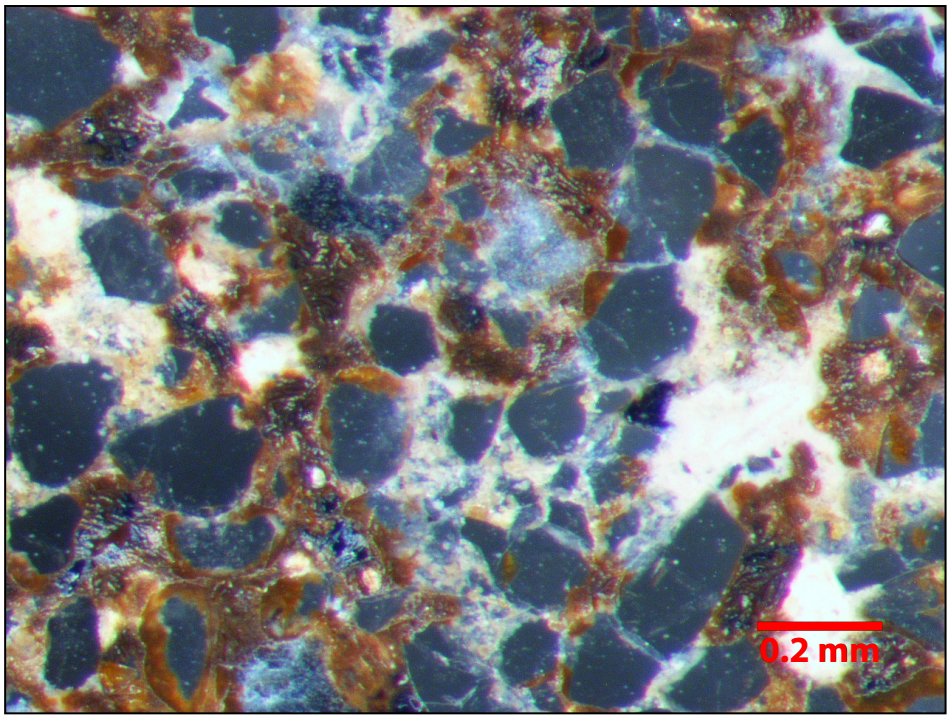

Figure A6–6. Reflected-light photomicrograph of sample RG-DL-20200722-17 (map label RG13).

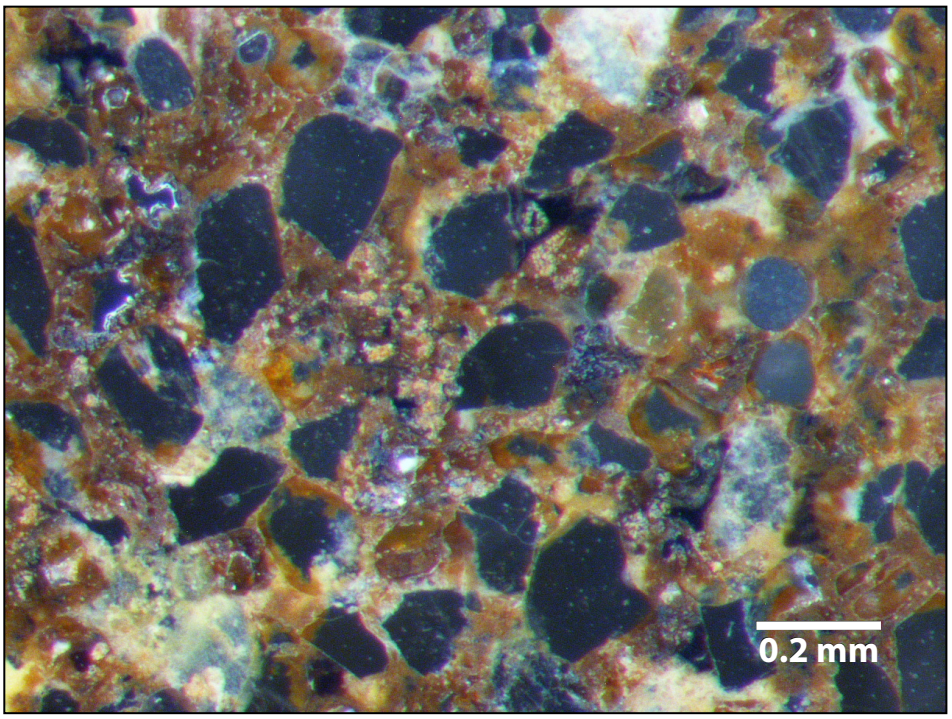

Figure A6–7. Reflected-light photomicrograph of sample RG-DL-20200722-18 (map label RG14).

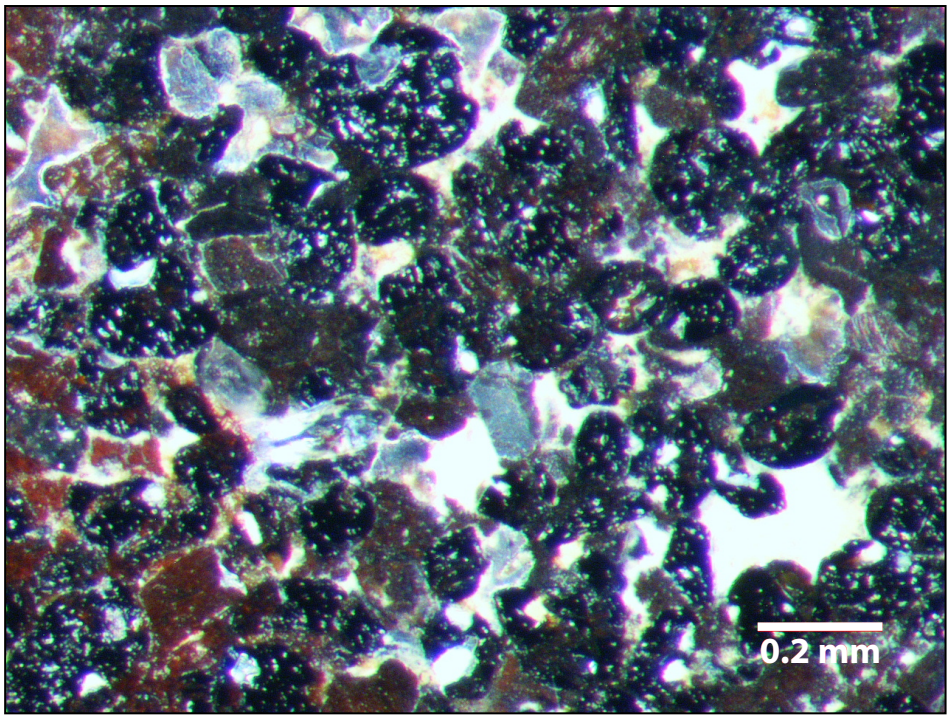

Figure A6–8. Reflected-light photomicrograph of sample RG-DL-20200722-20 (map label RG15).

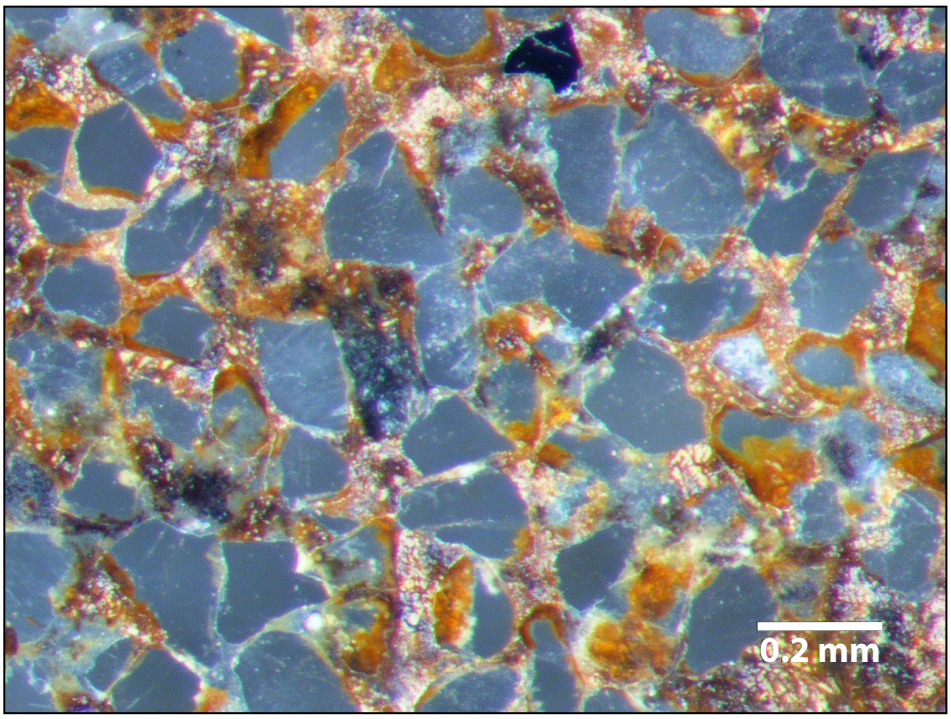

Figure A6–9. Reflected-light photomicrograph of sample RG-DL-20200722-21 (map label RG16).

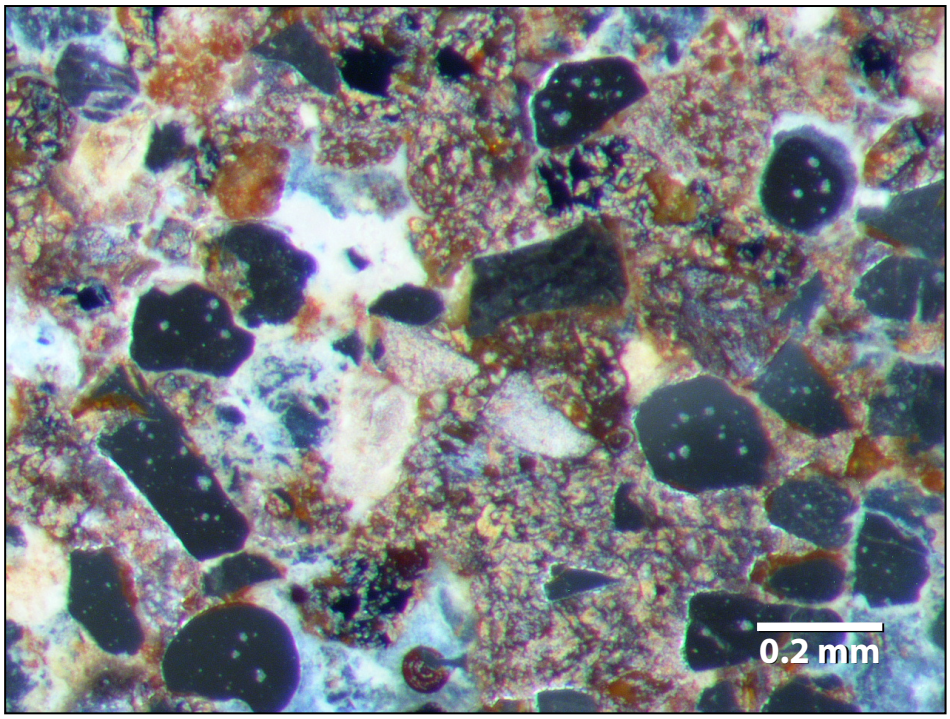

Figure A6–10. Reflected-light photomicrograph of sample RG-DL-20200722-22 (map label RG17).

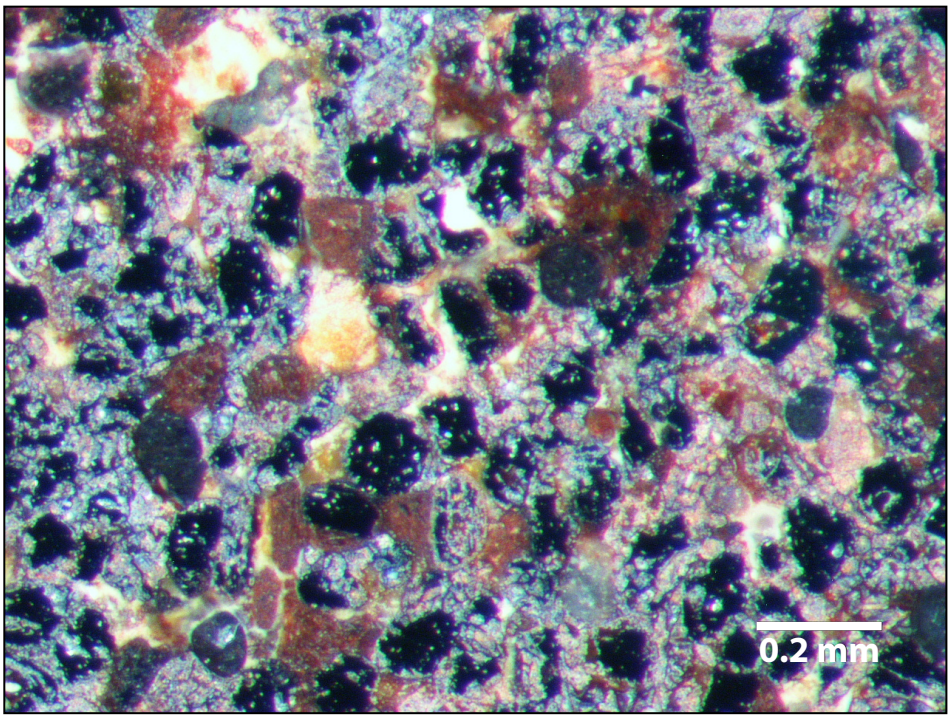

Figure A6–11. Reflected-light photomicrograph of sample RG-DL-20200722-23 (map label RG18).

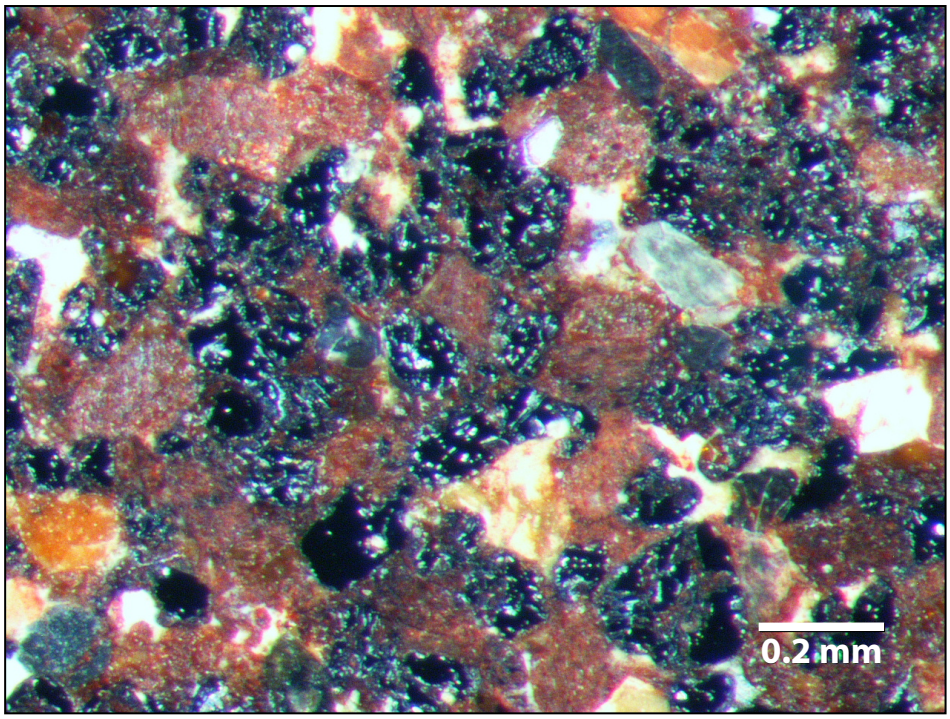

Figure A6–12. Reflected-light photomicrograph of sample RG-DL-20200722-24 (map label RG19).

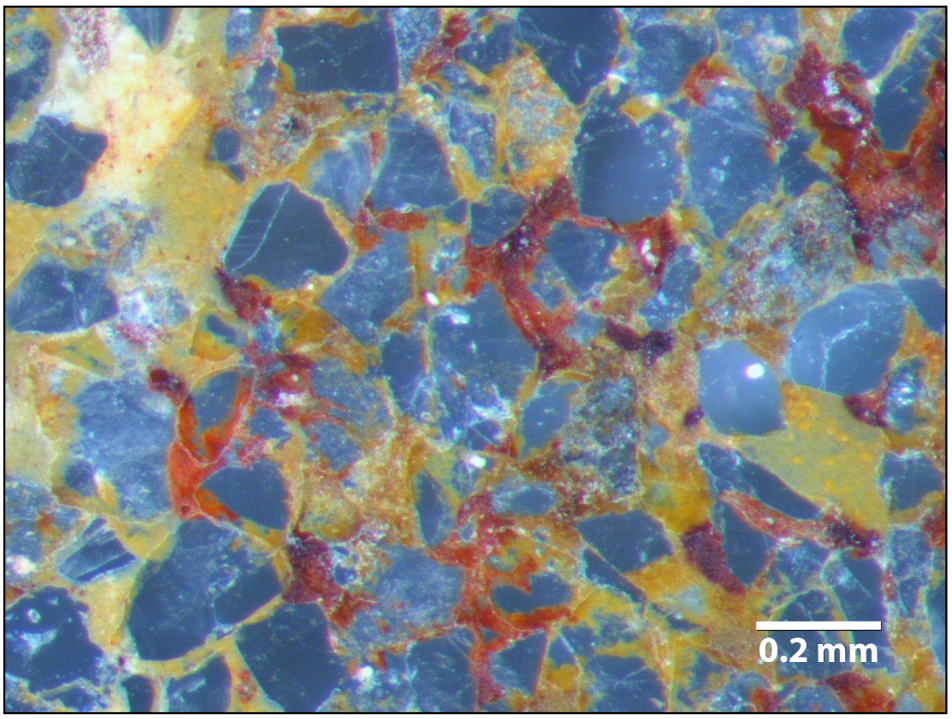

Figure A6–13. Reflected-light photomicrograph of sample RG-DL-20200722-25 (map label RG20).

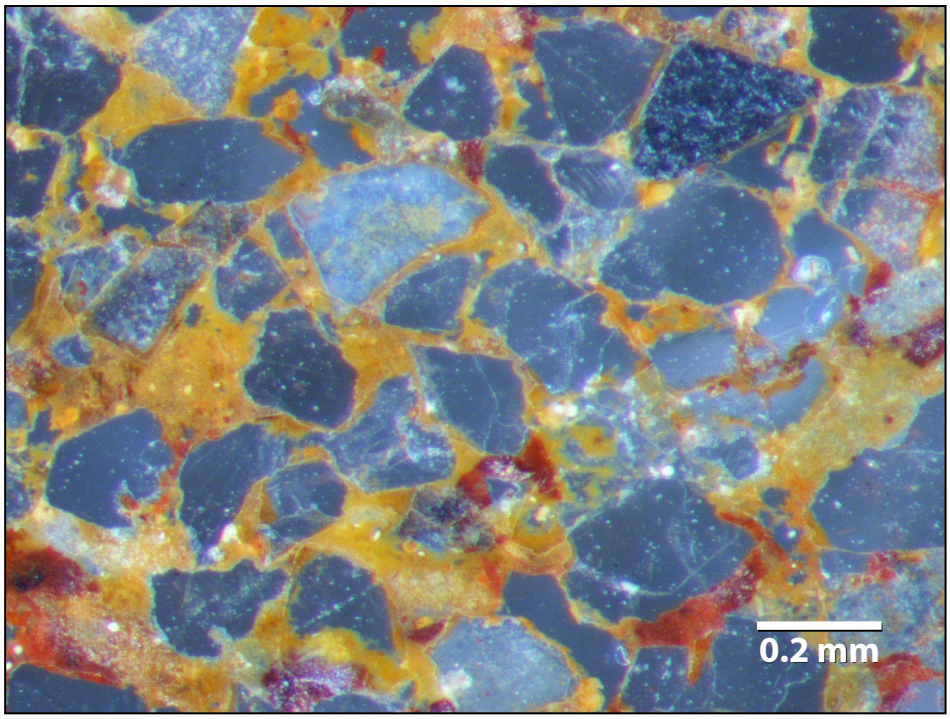

Figure A6–14. Reflected-light photomicrograph of sample RG-DL-20200722-26 (map label RG21).

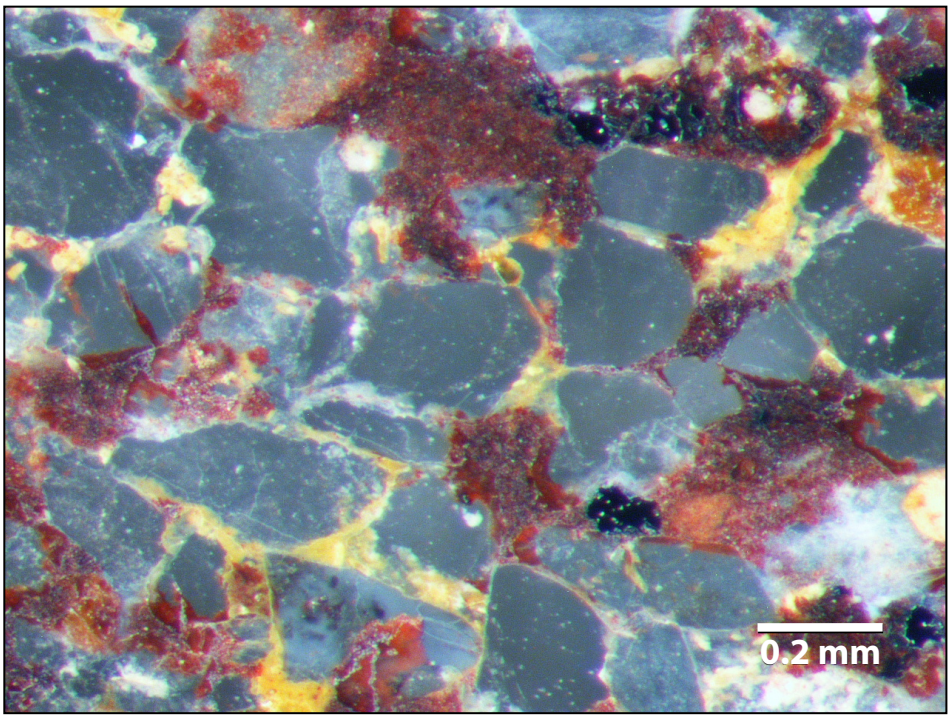

Figure A6–15. Reflected-light photomicrograph of sample RG-DL-20200722-27 (map label RG22).